The high polarisation of the X-rays from the Black Hole X-ray Binary 4U 1630–47 challenges standard thin accretion disc scenario

Ajay Ratheesh[1*], Michal Dovčiak[2], Henric Krawczynski[3], Jakub Podgorný[4,2,5], Lorenzo Marra[6], Alexandra Veledina[7,8], Valery Suleimanov[9], Nicole Rodriguez Cavero[3], James Steiner[10], Jiri Svoboda[2], Andrea Marinucci[11], Stefano Bianchi[6], Michela Negro[12,13,14], Giorgio Matt[6], Francesco Tombesi[15,16,17], Juri Poutanen[7], Adam Ingram[18], Roberto Taverna[19], Andrew West[3], Vladimir Karas[2], Francesco Ursini[6], Paolo Soffitta[1], Fiamma Capitanio[1], Domenico Viscolo[20,21], Alberto Manfreda[22], Fabio Muleri[1], Maxime Parra[23,6], Banafsheh Beheshtipour[3], Sohee Chun[3], Niccolò Cibrario[24,25], Niccolò Di Lalla[26], Sergio Fabiani[1], Kun Hu[3], Philip Kaaret[27], Vladislav Loktev[7], Romana Mikušincová[6], Tsunefumi Mizuno[28], Nicola Omodei[26], Pierre-Olivier Petrucci[23], Simonetta Puccetti[29], John Rankin[1], Silvia Zane[30], Sixuan Zhang[28], Iván Agudo[31], Lucio Antonelli[32,29], Matteo Bachetti[33], Luca Baldini[20,21], Wayne Baumgartner[27], Ronaldo Bellazzini[20], Stephen Bongiorno[27], Raffaella Bonino[24,34], Alessandro Brez[20], Niccolò Bucciantini[35,36,37], Simone Castellano[20], Elisabetta Cavazzuti[11], Chien-Ting Chen[38], Stefano Ciprini[16,29], Enrico Costa[1], Alessandra De Rosa[1], Ettore Del Monte[1], Laura Di Gesu[11], Alessandro Di Marco[1], Immacolata Donnarumma[11], Victor Doroshenko[9], Steven Ehlert[27], Teruaki Enoto[39], Yuri Evangelista[1], Riccardo Ferrazzoli[1], Javier Garcia[40], Shuichi

Gunji[41], Kiyoshi Hayashida[42], Jeremy Heyl[43], Wataru Iwakiri[44], Svetlana Jorstad[45,46], Fabian Kislat[47], Takao Kitaguchi[39], Jeffery Kolodziejczak[27], Fabio La Monaca[1], Luca Latronico[24], Ioannis Liodakis[48], Simone Maldera[24], Frédéric Marin[4], Alan Marscher[45], Herman Marshall[49], Francesco Massaro[24,34], Ikuyuki Mitsuishi[50], C.-Y. Ng[51], Stephen O'Dell[27], Chiara Oppedisano[24], Alessandro Papitto[32], George Pavlov[52], Abel Peirson[26], Matteo Perri[29,32], Melissa Pesce-Rollins[20], Maura Pilia[33], Andrea Possenti[33], Brian Ramsey[27], Oliver Roberts[38], Roger Romani[26], Carmelo Sgrò[20], Patrick Slane[10], Gloria Spandre[20], Douglas Swartz[38], Toru Tamagawa[39], Fabrizio Tavecchio[53], Yuzuru Tawara[50], Allyn Tennant[27], Nicholas Thomas[27], Alessio Trois[33], Sergey Tsygankov[7], Roberto Turolla[19,30], Jacco Vink[54], Martin Weisskopf[27], Kinwah Wu[30] and Fei Xie[55,1]

[1]INAF Istituto di Astrofisica e Planetologia Spaziali, Via del Fosso del Cavaliere 100, 00133 Roma, Italy.
[2]Astronomical Institute of the Czech Academy of Sciences, Boční II 1401/1, 14100 Praha 4, Czech Republic.
[3]Physics Department and McDonnell Center for the Space Sciences, Washington University in St. Louis, St. Louis, MO 63130, USA.
[4]Université de Strasbourg, CNRS, Observatoire Astronomique de Strasbourg, UMR 7550, 67000 Strasbourg, France.
[5]Astronomical Institute, Charles University, V Holešovičkách 2, CZ-18000, Prague, Czech Republic.
[6]Dipartimento di Matematica e Fisica, Università degli Studi Roma Tre, Via della Vasca Navale 84, 00146 Roma, Italy.
[7]Department of Physics and Astronomy, 20014 University of Turku, Finland.
[8]Nordita, KTH Royal Institute of Technology and Stockholm University, Hannes Alfvéns väg 12, SE-10691 Stockholm, Sweden.
[9]Institut für Astronomie und Astrophysik, Universität Tübingen, Sand 1, 72076 Tübingen, Germany.
[10]Center for Astrophysics ,Harvard & Smithsonian, 60 Garden St, Cambridge, MA 02138, USA.
[11]ASI - Agenzia Spaziale Italiana, Via del Politecnico snc, 00133 Roma, Italy.

[12]University of Maryland, Baltimore County, Baltimore, MD 21250, USA.
[13]NASA Goddard Space Flight Center, Greenbelt, MD 20771, USA.
[14]Center for Research and Exploration in Space Science and Technology, NASA/GSFC, Greenbelt, MD 20771, USA.
[15]Dipartimento di Fisica, Università degli Studi di Roma "Tor Vergata", Via della Ricerca Scientifica 1, 00133 Roma, Italy.
[16]Istituto Nazionale di Fisica Nucleare, Sezione di Roma "Tor Vergata", Via della Ricerca Scientifica 1, 00133 Roma, Italy.
[17]Department of Astronomy, University of Maryland, College Park, Maryland 20742, USA.
[18]School of Mathematics, Statistics, and Physics, Newcastle University, Newcastle upon Tyne NE1 7RU, UK.
[19]Dipartimento di Fisica e Astronomia, Università degli Studi di Padova, Via Marzolo 8, 35131 Padova, Italy.
[20]Istituto Nazionale di Fisica Nucleare, Sezione di Pisa, Largo B. Pontecorvo 3, 56127 Pisa, Italy.
[21]Dipartimento di Fisica, Università di Pisa, Largo B. Pontecorvo 3, 56127 Pisa, Italy.
[22]Istituto Nazionale di Fisica Nucleare, Sezione di Napoli, Strada Comunale Cinthia, 80126 Napoli, Italy.
[23]Université Grenoble Alpes, CNRS, IPAG, 38000 Grenoble, France.
[24]Istituto Nazionale di Fisica Nucleare, Sezione di Torino, Via Pietro Giuria 1, 10125 Torino, Italy.
[25]Dipartimento di Fisica, Universit'a degli Studi di Torino, Via Pietro Giuria 1, 10125 Torino, Italy.
[26]Department of Physics and Kavli Institute for Particle Astrophysics and Cosmology, Stanford University, Stanford, California 94305, USA.
[27]NASA Marshall Space Flight Center, Huntsville, AL 35812, USA.
[28]Hiroshima Astrophysical Science Center, Hiroshima University, 1-3-1 Kagamiyama, Higashi-Hiroshima, Hiroshima 739-8526, Japan.
[29]Space Science Data Center, Agenzia Spaziale Italiana, Via del Politecnico snc, 00133 Roma, Italy.
[30]Mullard Space Science Laboratory, University College London, Holmbury St Mary, Dorking, Surrey RH5 6NT, UK.

[31]Instituto de Astrofísica de Andalucía—CSIC, Glorieta de la Astronomía s/n, 18008 Granada, Spain.
[32]INAF Osservatorio Astronomico di Roma, Via Frascati 33, 00078 Monte Porzio Catone (RM), Italy.
[33]INAF Osservatorio Astronomico di Cagliari, Via della Scienza 5, 09047 Selargius (CA), Italy.
[34]Dipartimento di Fisica, Università degli Studi di Torino, Via Pietro Giuria 1, 10125 Torino, Italy.
[35]INAF Osservatorio Astrofisico di Arcetri, Largo Enrico Fermi 5, 50125 Firenze, Italy.
[36]Dipartimento di Fisica e Astronomia, Università degli Studi di Firenze, Via Sansone 1, 50019 Sesto Fiorentino (FI), Italy.
[37]Istituto Nazionale di Fisica Nucleare, Sezione di Firenze, Via Sansone 1, 50019 Sesto Fiorentino (FI), Italy.
[38]Science and Technology Institute, Universities Space Research Association, Huntsville, AL 35805, USA.
[39]RIKEN Cluster for Pioneering Research, 2-1 Hirosawa, Wako, Saitama 351-0198, Japan.
[40]California Institute of Technology, Pasadena, CA 91125, USA.
[41]Yamagata University,1-4-12 Kojirakawa-machi, Yamagata-shi 990-8560, Japan.
[42]Osaka University, 1-1 Yamadaoka, Suita, Osaka 565-0871, Japan.
[43]University of British Columbia, Vancouver, BC V6T 1Z4, Canada.
[44]International Center for Hadron Astrophysics, Chiba University, Chiba 263-8522, Japan.
[45]Institute for Astrophysical Research, Boston University, 725 Commonwealth Avenue, Boston, MA 02215, USA.
[46]Department of Astrophysics, St. Petersburg State University, Universitetsky pr. 28, Petrodvoretz, 198504 St. Petersburg, Russia.
[47]Department of Physics and Astronomy and Space Science Center, University of New Hampshire, Durham, NH 03824, USA.
[48]Finnish Centre for Astronomy with ESO, 20014 University of Turku, Finland.
[49]MIT Kavli Institute for Astrophysics and Space Research, Massachusetts Institute of Technology, 77 Massachusetts Avenue, Cambridge, MA 02139, USA.

[50]Graduate School of Science, Division of Particle and Astrophysical Science, Nagoya University, Furo-cho, Chikusa-ku, Nagoya, Aichi 464-8602, Japan.
[51]Department of Physics, The University of Hong Kong, Pokfulam, Hong Kong.
[52]Department of Astronomy and Astrophysics, Pennsylvania State University, University Park, PA 16802, USA.
[53]INAF Osservatorio Astronomico di Brera, Via E. Bianchi 46, 23807 Merate (LC), Italy.
[54]Anton Pannekoek Institute for Astronomy & GRAPPA, University of Amsterdam, Science Park 904, 1098 XH Amsterdam, The Netherlands.
[55]Guangxi Key Laboratory for Relativistic Astrophysics, School of Physical Science and Technology, Guangxi University, Nanning 530004, China.

*Corresponding author(s). E-mail(s): ajay.ratheesh@inaf.it;

Abstract

Large, energy-dependent X-ray polarisation is observed in 4U 1630–47, a black hole in an X-ray binary, in the high-soft emission state. In this state, X-ray emission is believed to be dominated by a thermal, geometrically thin, optically thick accretion disc. However, the observations with the Imaging X-ray Polarimetry Explorer (*IXPE*) reveal an unexpectedly high polarisation degree, rising from 6% at 2 keV to 10% at 8 keV, which cannot be reconciled with standard models of thin accretion discs. We argue that an accretion disc with an only partially ionised atmosphere flowing away from the disc at mildly relativistic velocities can explain the observations.

Keywords: polarisation, black holes, accretion disc, X-ray binaries

1 Introduction

Black hole X-ray binaries (BHXRBs) consist of a black hole (BH) accreting matter from a companion star. These systems provide opportunities to investigate the inner workings of accretion flows, including their thermal stability and the mechanisms of angular momentum transport, as well as the formation of relativistic outflows, winds and jets [1–3].

The X-ray polarisation observations (in the 2–8 keV range) conducted with the Imaging X-ray Polarimetry Explorer (*IXPE*, [4]), a NASA mission in collaboration with the Italian Space Agency (ASI), launched on December 9th 2021, are providing us with new significant insights into BHXRBs. In particular, the 4% polarisation observed for the archetypal BHXRB Cyg X-1 [5], parallel to the radio jet, constrained the geometry of hot corona, responsible for the power-law emission in the hard state, to be extended perpendicular to the jet direction (see [6, 7] for detailed descriptions of the different X-ray states). On the other hand, the much higher polarisation degree ($\sim$ 20%) observed for the black hole candidate Cyg X-3 in the hard state [8], with polarisation direction perpendicular to that of the discrete radio blobs, can be explained if radiation emitted by a highly luminous (but not directly visible) source is reflected off the funnel walls of obscuring matter.

In this paper we present results from spectro-polarimetric observations of the accreting black hole 4U 1630–47 with *IXPE*, accompanied by spectral observations with the *NICER* and *NuSTAR* missions. Whereas Cyg X-1 and Cyg X-3 were observed in the hard state, 4U 1630–47 was observed in the high-soft state. In this state, the emission is believed to originate from a geometrically thin, optically thick accretion disc ($h/r \ll 1$ for the scale height h of the disc at radius r) as multi-temperature black-body (BB) emission [9–12]. However, slim ($h/r \lesssim 0.4$) or thick discs ($0.4 < h/r \lesssim 1$) have been predicted to occur at high accretion rates [13]. The *IXPE* observations of 4U 1630–47 now allow us to weigh in on this distinction based on the additional information encoded in the energy resolved polarisation degree and polarisation direction.

4U 1630–47 is a transient low-mass X-ray binary (LMXB) system, initially discovered by the Uhuru satellite in 1969 [14, 15], that subsequently exhibited recurrent outbursts with a spacing of approximately 2–3 years [16, 17]. An accurate determination of the properties of the binary system has not been possible as yet due to the high line-of-sight (LOS) extinction [18, 19]. The mass of the black hole, distance to the binary system, and the inclination (angle between the binary axis and the LOS) are thus poorly constrained. Based on the dust scattering halo around the source, the distance is estimated to be between 4.7 to 11.5 kpc [20]. The inclination of the binary is believed to be $\sim 65°$, explaining the observations of X-ray dips but the absence of eclipses [16, 21] and the detection of Doppler shifted lines emitted by a jet [22]. The source shows evidence for a wind, believed to be equatorial [22–24]. The thermal component usually dominates the spectrum during outbursts [19, 25], making it an ideal candidate for investigating the properties of the disc.

We present the observational results in Sect. 2 and discuss the implications for the geometry of the accretion disc and the properties of the accretion disc photosphere in Sect. 3.

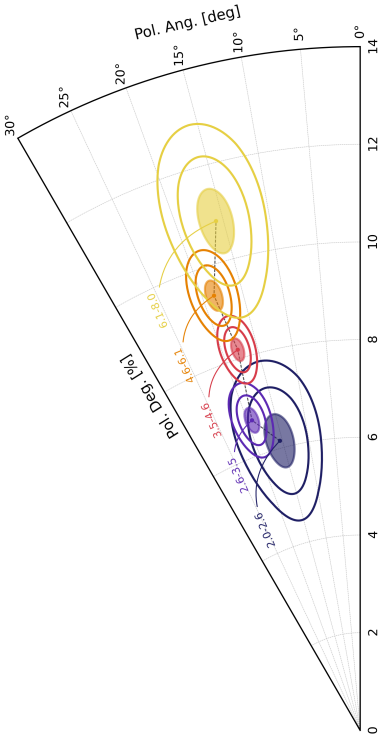

Fig. 1 Measured polarisation degree and angle of 4U 1630–47 as a function of the energy. The analysis is carried out using the publicly available version of `ixpeobssim` [26]. The shaded region and ellipses shows the 68%, 95%, and 99.7% confidence interval results.

2 Observational Results

Daily monitoring of 4U 1630–47 by the Gas Slit Camera (GSC) onboard Monitor of All-sky X-ray Image (*MAXI*, [27]) showed an increase in the count rate, suggesting an outburst from the source in 2022 July [28] (Figure M1). During this outburst, *IXPE* performed a target of opportunity (ToO) observation starting on 2022 August 23 and ending on 2022 September 2, for a total exposure of approximately 460 ks, along with continuous spectral monitoring from the Neutron Star Interior Composition Explorer (*NICER*, [29]) and the Nuclear Spectroscopic Telescope Array (*NuSTAR*, [30]).

Linear polarisation was detected with a statistical confidence of around 50σ (Figure 1). The 2–8 keV polarisation degree (PD) and position angle (PA), measured east of North, are $8.32 \pm 0.17\%$ and $17.8° \pm 0.6°$, respectively (the uncertainties are reported at 68% confidence level). Whereas PD increases from approximately 6% at 2 keV to 10% at 8 keV, the polarisation direction stays constant with energy within the statistical accuracy of the measurements (bottom right panel on Figure 2). The radio jet from this source has never been

resolved, leaving us without a jet direction to compare the X-ray polarisation to.

The *NICER* data reveal a featureless power density spectrum with fractional variability of less than 5% Root Mean Square (RMS) and a high disc temperature of ~ 1.4 keV, showing that the source was in the high-soft state. The *NICER* energy spectra exhibit blue-shifted absorption lines, with outflow velocities $\approx 0.003\,c$ (with c the speed of light), suggesting the existence of equatorial disc wind outflows.

We fitted the combined, quasi-simultaneous *NICER* and *NuSTAR* data with a thin disc model. The best fit value for the BH mass is very large, $60\,M_{\odot}$ (Methods, Table M1), already suggesting a problem with this model. The combined *NICER* and *NuSTAR* energy spectra reveal a weak power law component, contributing approximately 2-3% of the energy flux in the *IXPE* 2–8 keV energy range. The photon index was highly variable, exhibiting values between 2.8 and 4.8 (see Methods) consistent with the soft state of BHXRBs [6, 31]. We do not find evidence for a broad reflection feature, as reported in [23, 32].

3 Implications for the accretion disc geometry and accretion disc photosphere

The high and energy-dependent PD of 4U 1630−47, increasing from 6% at 2 keV to 10% at 8 keV, cannot be explained in the framework of the standard thin disc model. In this model, the polarisation of the thermal emission emerging from the disc should roughly follow Chandrasekhar's classical result for a semi-infinite free electron scattering atmosphere [33]. Polarisation degree of emission reaching the observer tends to be significantly lower than Chandrasekhar's results, owing to two effects. As the polarisation vector is parallel transported as the photons propagate through curved space-time, the polarisation direction projected onto the sky changes. The competing polarisation directions of the emission from different parts of the disc partially cancel [34, 35]. Furthermore, emission following the space-time curvature can return to the disc and scatter off it. The polarisation of the direct and reflected returning emission again partially cancel [36, 37]. The Chandrasekhar formula can produce X-rays with PD $\gtrsim 6\%$ in the disc rest-frame for viewing angles exceeding 80° (Methods, Figure M4). However, de-polarisation by relativistic effects means that the standard model cannot reproduce the observed PD for any inclination angle (left panel on Figure 2). Moreover, the observed increase of PD with energy cannot be reproduced in the disc rest-frame, since electron scattering is energy independent.

Considering instead scattering from free and bound electrons in a partially-ionised plasma increases the predicted PD in the disc rest-frame from the pure electron scattering case (Methods, Figure M4), and also in principle enables an increase of PD with energy (Methods, Figure M5). This is because the

absorption processes lead to a higher fraction of the escaping photons travelling perpendicular to the disc plane, plus these photons scatter on average fewer times [38]. Radiative transfer calculations of a plane-parallel, partially-ionised slab in photo-ionisation equilibrium [38, 39], extensively discussed in the Methods, predict a PD in the disc rest-frame increasing from $\sim 6\%$ at 2 keV to $\sim 10\%$ at 8 keV (as is observed by *IXPE*), as long as the slab is highly ionised and viewed from an angle of $\sim 84°$. The former condition is met for black-body temperatures $kT_{\rm BB} \gtrsim 0.5$ keV, high slab optical thickness, τ, of up to 10, and for a wide range of slab densities, $n({\rm H}) \sim 10^{12-20}$ cm^{-3} (Figs. M5–M7 in Methods). In this scenario, the polarization angle should be parallel with the disc. However, verifying this is currently impossible due to the lack of constraints on the orientation of the radio jet. Once again general relativistic effects reduce the predicted observed PD in the *IXPE* energy band to well below the observed values (Figure M9, and Figure M11, right panel).

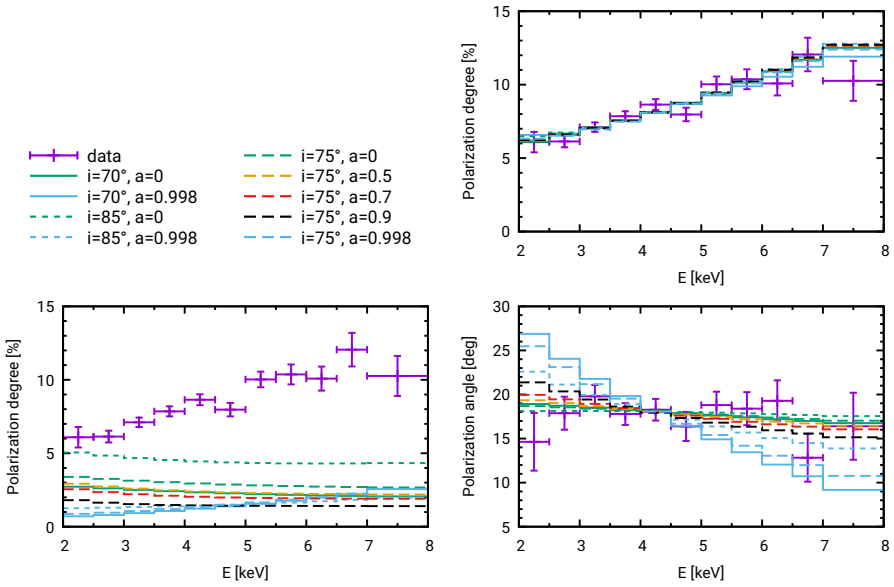

Fig. 2 Comparison of the observed (purple points with 68% confidence level error bars) and modelled 4U 1630−47 polarisation properties (different lines). The standard Novikov-Thorne geometrically thin accretion disc model with emission and reflection according to Chandrasekhar's pure scattering atmosphere model significantly under-predict the PDs (left). The results of thin disc models with an outflowing partially ionised photosphere can explain the data for low spins ($a = 0$ or 0.5) and $i = 70°$ or 75° inclinations (top right and bottom right). All models shown here assume optical thickness around 7. The models of the centre and lower panels assume an outflow velocity of $v \sim 0.5\,c$.

The relativistic corrections are significantly altered when we allow for relativistic vertical motion of the particles in an outflowing disc atmosphere. The model predicts higher PDs as the photons reaching the observers were emitted under larger inclinations with larger PDs. These photons reach the observer

owing to relativistic beaming effects. When we include this extra effect into the partially-ionised slab model, we can explain the observed PD and PA (right panels of Figure 2) with the combination of a low black hole spin ($a \lesssim 0.5$), and a highly-ionised atmosphere with large optical depth ($\tau \sim 7$) outflowing perpendicular to the accretion disc with a velocity $v \sim 0.5\,c$. The observed PD variability (see Figure M3 in Methods) could then be explained by changes in the optical depth or due to varying outflow velocity of such an atmosphere. In this picture, the absorption lines imprinted on the spectrum with blue shift velocity $v \sim 0.003$ c originate from an equatorial wind located further from the disc than the rapidly outflowing atmosphere. It is plausible that this is the same material; i.e. the outflow is initially rapid and dense at the disc surface before spreading and slowing down at larger distances, like in the case of Magneto-hydrodynamic (MHD) winds [40–44]. Such MHD wind models have been previously used to explain the blue-shifted absorption lines in this source [45].

The modelling described in the Methods sections shows that geometrically thicker discs, such as the slim disc [13] or recently very popular puffy discs [46], can lead to increased PDs, and to PDs increasing with energy. However, for the considered disc geometries, even our most optimistic fine tuning of the model parameters (black hole spin, inclination of the observer, disc thickness) cannot fully reproduce the observed high PDs. We cannot exclude here that the high PDs may be explained with other disc geometries that increase the fraction of scattered X-rays even more.

The high inclination could also be explained by a scenario where the inner accretion flow is more inclined than the binary system, like in the case of a wrapped disk. If the BH spin axis is not aligned with the binary orbital axis, the gravitational effects can result in the inner accretion flow becoming aligned perpendicular to the BH spin axis, potentially leading to a greater inclination of the inner disk [47].

During the writing of this work, two other groups independently analysed the same *IXPE* data sets [48, 49], obtaining observational results consistent with those presented in this work. The authors posit that the high polarisation degree can be explained by scattering off a wind. We find that reflection off a highly ionised wind via Thomson scatterings leads to rather constant PDs [8, 50], contrary to what is observed. For the reflected flux to make a significant contribution to the total spectrum, the solid angle subtended by the wind on the X-ray source needs to be greater. Reflection off a distant wind (rather than off the hot inner portion of the accretion disc) should furthermore give rise to emission lines [37], which we do not see in the *NICER* and *NuSTAR* energy spectra. Further, using our *NuSTAR* data we constrain the Comptonised power-law, and hence confirm its negligible contribution in the 2-8 keV band.

We conclude that the new observational diagnostics provided by *IXPE*, PD and PA of the X-ray radiation, imply significant deviations from the standard thin disc model. We show that a thin disc with an outflowing atmosphere and

with significant absorption effects can explain the observations. Additional observations of the source in the same emission state at different flux levels and in different emission states will constrain the accretion disc geometry and properties even further.

Methods

Data sets and data reduction

IXPE: The Imaging X-ray Polarimetry Explorer (*IXPE*) consists of three independent telescopes, each made up of a Mirror Module Assembly (MMA) and a detector unit (DU) [4, 51–53]. *IXPE* observed 4U 1630–47, from 2022 August 23 23:14 to 2022 September 02 18:54, for a total effective exposure of approximately 463 ks. The analysis of the *IXPE* data is performed using `ixpeobssim` software, version 28.4.0 [26], which is based on level-2 processed data. For our analysis, we used the combined data sample collected by the three identical detector units, with appropriate rotation to align them with the same reference system in sky coordinates. We utilised SAOImage DS9 software [54] for the source and background region selection process. The source region was chosen as a circular area with a radius of $1.0'$, centred at the region of maximum intensity within the field of view, consistent with the source location. The background region was defined as a concentric annulus with an inner radius of $2.5'$ and an outer radius of $4.3'$. The `ixpeobssim` routine `xpselect` was used to create the source and background event files.

The polarisation degree and angle were computed using the `xpbin` routine of `ixpeobssim`, using the flag `--algorithm PCUBE`. Version 11 of the *IXPE* response functions was used to process the data. This approach enabled the calculation of the polarisation properties in a model-independent manner. The `xpbin` routine allows us to perform a background subtraction from source and background files: note that the source-emission leakage into the background region does not affect the final source polarisation estimation significantly. Then we have generated the OGIP standard FITS files of polarisation degree and angle together with the unit response files with the `flx2xsp` tool from the `HEASOFT` package [55] so that we can directly feed them to `XSPEC` in order to perform polarimetric fits [56]. The `xpselect` and `xpbin` routines were also used to generate event files for the analysis of variability over time.

NICER: NICER uses 52 silicon drift detectors (SDDs), each with a paired single-scattering concentrator optic and mutually aligned on the sky [57]. *NICER* is sensitive in the 0.2–12 keV range, offering < 100 ns time resolution, and has a peak effective area ~ 2000 cm^2. *NICER* carried out 11 observations of 4U 1630–47 during the *IXPE* campaign, from 2022 August 22 to 2022 September 1. A total of 64 GTIs have been used for our science analysis, for an aggregate time of ≈ 27 ks and a total of > 11 million X-ray counts.

NICER data were reduced and processed with the version 9 of the *NICER* data analysis software `NICERDAS`. Data were filtered following standard practices, but allowing data from South Atlantic Anomaly (SAA) passages. For each GTI, data from detectors 14, 34, and 54 were excised owing to calibration problems among this subset. Additionally, the average rates of overshoot, undershoot, and X-ray events per GTI were assessed, and any detector which

> 15 median absolute deviation (MAD) was excluded for that GTI. All exposure times were corrected for the detector dead time ($< 1\%$). The background spectra were computed using the 3C 50 background model [58]. Only GTIs of length $t > 60$ s and for which the background rate was 100 times below the source rate were used for the analysis. A total of 27 ks of simultaneous *NICER* observations were finally available for the analysis. The spectral and lightcurve files were extracted from the event files using `XSELECT` version 2.5b and the response files were generated using `nicerarf` and `nicerrmf`.

NUSTAR: 4U 1630–47 was observed three times by *NuSTAR* during the *IXPE* pointing (on 2022 August 25 and 29, and on 2022 September 1) using the two co-aligned X-ray telescopes, each with a corresponding Focal Plane Module A (FPMA) and B (FPMB) [30]. The total elapsed times of the three snapshots are 38.3 ks, 31.6 ks and 32.5 ks, respectively. The Level 1 data products were processed with the *NuSTAR* Data Analysis Software (`NuSTARDAS`) package (v. 2.1.2). Cleaned event files (level 2 data products) were produced and calibrated using standard filtering criteria with the `nupipeline` task and the *NuSTAR* calibration files 20220510 available in the CALDB database. Extraction radii for the source and background spectra were $60''$. The spectra and lightcurves were then generated by the `nuproducts` routine of the `NuSTARDAS` package. FPMA and FPMB spectra were binned following the procedure described in [59] and, in order to have a signal to noise ratio (SNR) greater than 3 in each spectral channel, the same energy binning was applied to the FPMB spectra. The net observing times for the FPMA and the FPMB data sets are 16.3 ks/16.6 ks, 13.2 ks/13.4 ks and 14.8 ks/15.0 ks for the three sets of *NuSTAR* data, respectively.

Detailed results from *IXPE*, *NICER*, and *NuSTAR*

Light curves: The top panel of Figure M1 shows the X-ray activity of the source between MJD 59700 (2022 May 1) and MHD 59900 (2022 November 17) monitored by *MAXI* mission. The 200-day interval includes the time period of the *IXPE* observation campaign. The source was detected in the high-soft state. The bottom panel shows the *IXPE*, *NICER*, and *NuSTAR* 2–8 keV, 1–10 keV, and 3–79 keV fluxes, respectively. The fluxes varied by ∼10% below 10 keV and by 15-20% above 10 keV. The source flux was thus rather stable during the campaign.

Spectral fit with *NICER* and *NuSTAR*

As 4U 1630−47 is highly variable (see Figure M1) we fitted the *NICER* and *NuSTAR* energy spectra selecting quasi-simultaneous data sets. From the set of *NICER* observations, we used data with the observational IDs 5501010104, 5501010108 and 5501010111 that match the same periods covered by *NuSTAR* observations with the observational IDs 80802313002, 80802313004 and 80802313006, respectively. We further denote these 3 observations as Obs

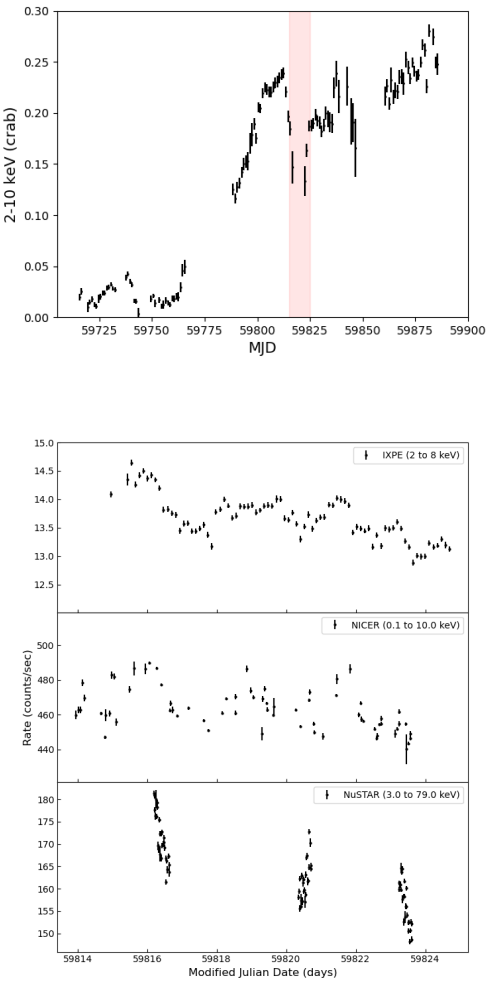

Fig. M1 Top: *MAXI* 2–10 keV light curves in one-day bins. The shaded red region indicates the time period of the *IXPE* observation campaign. Bottom: *IXPE*, *NICER* and *NuSTAR* lightcurves in the 2–8 keV, 0.1–10 keV and 3–79 keV bands, respectively, during the *IXPE* campaign. The *IXPE* light curve gives the combined count rates of all three Detector Units (DUs), whereas for *NuSTAR* only the light curve obtained from Focal Plane Module A is shown.

1, Obs 2 and Obs 3, respectively. For the spectral analysis, we used only *NICER* data with low background radiation (we avoided here data during SAA passage).

We employed a model consisting of thermal accretion-disc emission accounting for relativistic effects (KERRBB, [60]), the Comptonised emission (NTHCOMP, [61, 62]), ionised absorber modelled with `CLOUDY` (`cloudy`, [63])

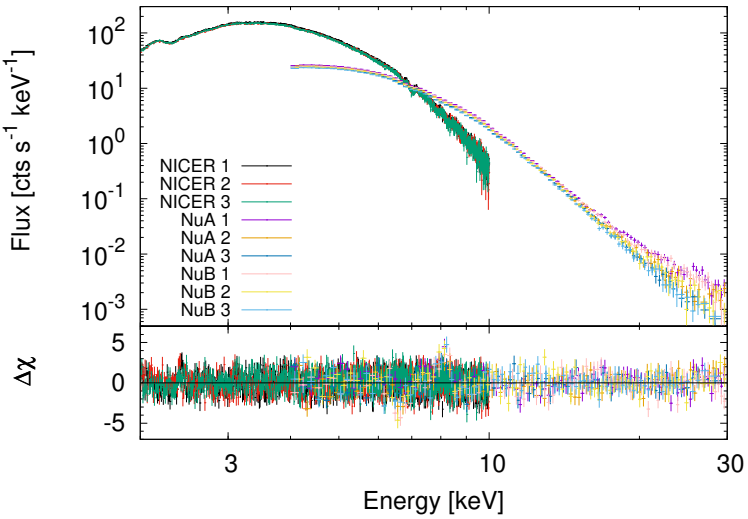

Fig. M2 Spectral fit of simultaneous data from *NICER* and *NuSTAR* using a model consisting of thermal accretion-disc emission (SLIMBH), Comptonised emission (NTHCOMP), ionised absorber (CLOUDY), cold absorption (TBABS) and edges accounting for the instrumental features. The upper panel shows the spectra, the data residuals from the model ($\Delta\chi$ values) are shown in the bottom panel.

and cold absorption (TBABS, [64]), accounting for Galactic as well as local absorption. The `CLOUDY` absorption table reproduces the absorption lines self consistently through a slab with a constant density of 10^{12} cm^{-3} and a turbulence velocity of 500 km s^{-1}, illuminated by the unabsorbed intrinsic best fit SED described below. Modelling the absorption lines requires a highly ionised outflowing plasma, i.e. with ionisation parameter $\xi \sim 10^5$, and with a column density $N_{Heq} \sim 10^{24}$ cm^{-2}. The seed photons for NTHCOMP model are assumed to be from the multicolour disk black-body emission (inp_type parameter = 1) and we fixed the temperature to $kT_{\rm bb} = 1.47$, which resulted from initial fitting using DISKBB.

We further added an empirical EDGE model to account for the instrumental features at $\approx$ 2–3 keV in the *NICER* spectra and at $\approx$ 10 keV in the *NuSTAR* spectra. The gold M edge in the *NICER* spectra is a well known instrumental feature. We fixed the energy of the edge to the value $E = 2.4$ keV, as reported by [65] in the analysis of MAXI J1820+070 *NICER* spectra. The origin of the $\approx$ 10 keV edge in the *NuSTAR* spectra is less known, but it was observed in other sources as well (e.g. the analysis of LMC X-1, [66]). We added a reflection component, a second Comptonisation component, or a second ionised absorption to the model, but none of these components improved the overall fit or the residuals in this part of the *NuSTAR* spectrum. We, therefore, modelled it with the empirical EDGE model. Finally, we accounted for absolute calibration uncertainties between *NICER* and *NuSTAR* instruments allowing for a

Table M1 Spectral fit results for different fixed values of black hole spin and inclination with the KERRBB model.

Inclination	Spin	Mass	Accretion rate	Fit goodness
i (deg)	a	$M_{\rm bh}$ ($M_\odot$)	$M_{\rm dd}$ (10^{18} g s^{-1})	χ^2 (2935 dof)
70	0.7	$9.98^{+0.06}_{-0.08}$	$3.9 - 4.3$	4693
	0.998	$29.8^{+0.02}_{-0.02}$	$0.99 - 1.09$	3585
85	0.7	$16.1^{+0.01}_{-0.01}$	$8.3 - 8.9$	3711
	0.998	$59.8^{+0.04}_{-0.02}$	$1.02 - 1.12$	3563

Table M2 Spectral fit parameters to simultaneous *NICER* and *NuSTAR* observations with the SLIMBH model.

Comp.	Parameter (unit)	Description	Obs 1	Obs 2	Obs 3
TBabs	$N_{\rm H}$ (10^{22} cm^{-2})	H column density	$7.92^{+0.07}_{-0.02}$	$7.94^{+0.02}_{-0.02}$	$7.85^{+0.02}_{-0.02}$
CLOUDY	$\log \xi$	ionisation	$5.13^{+0.06}_{-0.04}$	$5.01^{+0.09}_{-0.03}$	$4.95^{+0.07}_{-0.04}$
	$\log N_{Heq}$	H column density	$24.03^{+0.02}_{-0.02}$	$24.03^{+0.03}_{-0.01}$	$24.04^{+0.03}_{-0.02}$
	z	Redshift	$-0.0002^{+0.0001}_{-0.0002}$	$-0.003^{+0.001}_{-0.001}$	$-0.003^{+0.001}_{-0.001}$
SLIMBH	$M_{\rm bh}$ ($M_\odot$)	Black hole mass		$18.0^{+0.7}_{-1.2}$	
	a	Black hole spin		$0.71^{+0.03}_{-0.14}$	
	$L_{\rm Edd}$	Luminosity	$0.53^{+0.03}_{-0.03}$	$0.51^{+0.02}_{-0.02}$	$0.49^{+0.02}_{-0.02}$
	i (deg)	Inclination		$85^{\rm f}_{-1.4}$	
	α	Viscosity		0.1 (frozen)	
	$D_{\rm bh}$ (kpc)	Distance		11.5 (frozen)	
	hd	Hardening factor		-1 (frozen)	
	$l_{\rm flag}$	Limb-darkening		0 (frozen)	
	$v_{\rm flag}$	Self-irradiation		0 (frozen)	
	norm	normalisation		1 (frozen)	
NTHCOMP	Γ	Photon index	$2.6^{+0.2}_{-0.2}$	$3.6^{+0.2}_{-0.2}$	$4.5^{+0.2}_{-0.2}$
	$kT_{\rm e}$ (keV)	Electron temp.		500 (frozen)	
	$kT_{\rm bb}$ (keV)	Seed photon temp.		1.47 (frozen)	
	norm (10^{-2})	normalisation	$2.6^{+1.1}_{-0.7}$	$6.3^{+1.8}_{-1.7}$	13^{+3}_{-3}
χ^2 / dof				3494/2933	

Note: The final model also included cross-calibration uncertainties between *NICER*, *NuSTAR A* and *B* instruments, modelled by MBPO model with $\Delta\Gamma = -0.101 \pm 0.008$ and normalisation $N_{\rm mbpo} = 1.16 \pm 0.02$ (consistent for both *NuSTAR A* and *B* instruments), and the instrumental edges with $E = 2.4$ keV and maximum $\tau = 0.074 \pm 0.005$ for *NICER* and $E = 9.7 \pm 0.1$ keV and maximum $\tau = 0.056 \pm 0.006$ for *NuSTAR*. See the main text for more details.

small discrepancy in the spectral slope and normalisation between the instruments using MBPO model, see [5]. With this model, we obtained the best fits for black hole spins $a \gtrsim 0.99$, inclinations $i \approx 85$ deg, and black hole masses $M_{\rm bh} \gtrsim 50 M_\odot$ (Table M1, last line) with a χ^2/dof = 3563/2937. The mass is much higher than estimated from previous analysis by [67] ($\approx 10 M_\odot$).

As the black hole mass, spin, inclination, and the distance in the KERRBB model are degenerate, we fixed the distance of the source to the value $D_{\rm bh} = 11.5$ kpc [20]. A smaller $D_{\rm bh}$ of 4.7 kpc is not excluded and would lead to a significantly smaller black hole mass and accretion rate, e.g. for spin $a = 0.97$ and inclination $i = 75°$, the best-fit black hole mass is $M_{\rm bh} \approx 26 M_\odot$ and $M_{\rm bh} \approx 12 M_\odot$, and the effective accretion rate $M_{\rm dd} \approx 1.8 \times 10^{18}$ g s^{-1} and $M_{\rm dd} \approx 0.3 \times 10^{18}$ g s^{-1} for $D_{\rm bh} = 11.5$ kpc and $D_{\rm bh} = 4.7$ kpc, respectively. The best-fit value of the black hole mass is also impacted by the value of spin and inclination. Table M1 shows the mass and accretion rate results obtained with KERRBB for a fixed distance $D_{\rm bh} = 11.5$ kpc, but for different sets of spin

and inclination values. The goodness of the fit clearly shows the preference towards high mass.

In the next step, we replaced the KERRBB by SLIMBH model [68] that accounts for a vertical structure of the disc using the code TLUSTY [69], which is especially important for higher accretion rate and luminosity $L > 0.3\,L_{\rm Edd}$ when conditions for the razor-thin standard accretion disc model are not fulfilled and a very large hardening factor is required to fit the spectra well [70]. The best-fit model describes the data with a $\chi^2/{\rm dof} = 3494/2933$, see Figure M2 and Table M2. To calculate the χ^2 values, we used model weighting. The reduced chi-squared value $\chi^2_{\rm red} = \chi^2/{\rm dof} \lesssim 1.2$ provides a very good fit, given the fact that we have not applied any systematics to the data that would account for uncertainties in instrument calibration between *NICER* and *NuSTAR* (that can be within a few percent) as well as possible spectral variability within the individual exposures since the data acquired by the two missions were not strictly simultaneous.[1] Variable absorption lines are also a contributing factor to the chi-square in the joint spectral fits of NICER and NuSTAR. However, as it falls outside the main scope of our study, we did not delve into investigating this aspect in detail. It is noteworthy that these lines do not significantly impact the crucial continuum parameters in our analysis. The fit requires a black hole mass of $\sim 18\,M_\odot$ and a black hole spin of $a \sim 0.7$, parameters which are more in line with expectations [67]. The luminosity is $L \approx 0.5\,L_{\rm Edd}$, i.e. already in the range when the slim disc approximation is more appropriate than the geometrically thin disc model. The soft X-ray spectrum is dominated by the thermal accretion disc emission. *NuSTAR* data revealed a variable Comptonisation component, which is best visible in a variable tail at very high energies ($\approx$ 15–30 keV). The photon index varies in the range $\Gamma \approx 2.8$–4.8, while the soft X-ray spectrum varies only little. In the 2–8 keV energy range, the Comptonisation contributes $2-3\%$ and is almost negligible in the soft X-ray band analysis.

Time averaged and time resolved spectro-polarimetric analysis

Table M3 gives the *IXPE* polarisation results for the entire *IXPE* data set. We investigated the time evolution of the spectral and polarimetric properties in one-day bins. Here, we characterise the thermal component by its maximum temperature and its normalization. Therefore we base the spectral analysis on fitting the 2–10 keV *NICER* data with the multiple temperature blackbody disc model (EZDISKBB, [71]). We use the same `CLOUDY` model as in the main spectral fit to model the absorption lines. We neglect the <2 keV data as absorption strongly suppresses the low-energy flux. The thermal model gives a good fit, as the power law component contributes only 2-3% to the 2–10 keV flux. The results of the analysis are shown in Figure M3. Whereas the maximum disc temperature stayed rather constant around ~ 1.4 keV, the flux

[1] While we have restricted the *NICER* data to be within the *NuSTAR* observations, we did not do that vice versa, since the statistics of such restricted *NuSTAR* data would be too low.

Table M3 polarisation degree and angle at different energy ranges across the *IXPE* energy band.

Energy range (keV)	PD (%)	PA (°)
2.0-2.5	6.1 ± 0.7	14.56 ± 3.3
2.5-3.0	6.13 ± 0.4	17.84 ± 1.89
3.0-3.5	7.11 ± 0.32	19.77 ± 1.29
3.5-4.0	7.85 ± 0.34	17.78 ± 1.24
4.0-4.5	8.66 ± 0.37	18.27 ± 1.23
4.5-5.0	7.96 ± 0.46	16.33 ± 1.66
5.0-5.5	10.02 ± 0.53	18.79 ± 1.53
5.5-6.0	10.39 ± 0.68	18.43 ± 1.88
6.0-6.5	10.11 ± 0.82	19.29 ± 2.33
6.5-7.0	12.05 ± 1.15	12.82 ± 2.73
7.0-7.5	9.26 ± 1.58	14.34 ± 4.88
7.5-8.0	11.8 ± 2.45	18.88 ± 5.95

normalisation varied between 35 and 40. The normalisation is given by the expression $f^{-4}\,(R_{\rm in}/D)^2\,\cos i$ with f being the spectral hardening factor, $R_{\rm in}$ the inner radius of the disc in km, D the source distance in 10 kpc, and i the disc inclination. The polarisation degree shows significant variability. Fitting a constant model to the *IXPE* results gives a χ^2 of 34.9 for 9 degrees of freedom (chance probability $6{\times}10^{-5}$).

Theoretical modelling of the spectro-polarimetric results

Analytical results

The observed high X-ray polarisation of 4U 1630–47 in the 2–8 keV energy band can be achieved if the system is viewed at a high inclination angle. The classical results of the pure electron-scattering, semi-infinite atmospheres [72, 73] show that the observed polarisation degree can be achieved for binary inclinations $\gtrsim 85°$, see Figure M4.

At such high inclinations the X-ray source becomes obscured by the outer parts of the accretion disc, for which an opening angle $\sim 12°$ has been observed [74]. Furthermore, for the source at inclination $> 80°$ complete eclipses are expected, but they have not been detected in this source.

However, as we note in the main text, the basic assumption of this model, namely, the complete ionisation of matter in the accretion disc atmosphere, is hard to achieve. For a fractional ionisation, absorption effects may significantly enhance the polarisation degree of escaping spectra [75, 76]. The parameter governing the polarisation degree is the ratio of scattering coefficient to the sum of scattering and true absorption coefficients, λ. Smaller values of λ tend to give higher polarisation degree. The presence of internal sources distributed within the disc atmosphere decreases the polarisation degree as compared to the classical Milne problem [77], where all the photons originate from the bottom of the atmosphere (at infinite optical depth) [78]. Nevertheless, the net polarisation degree in these cases can be higher than that in the pure electron-scattering atmosphere case (Figure M4), hence the lower limit on the

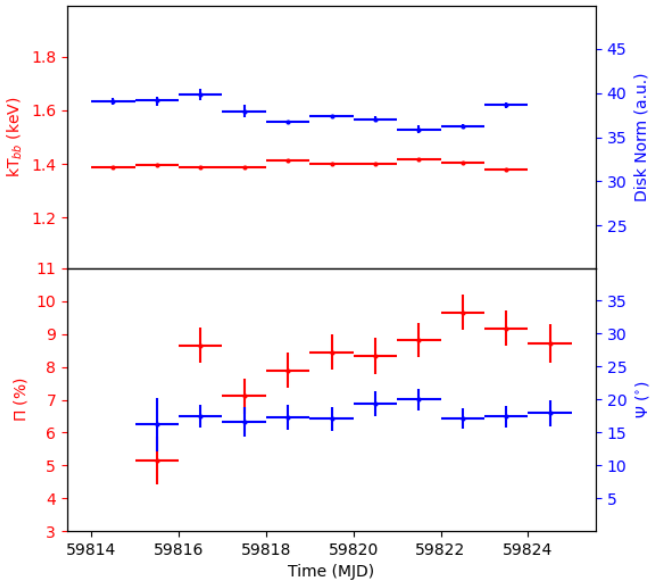

Fig. M3 The temporal variability of disc spectral parameters derived from *NICER* and polarimetric parameters derived from *IXPE* observations. Top: The inner disc temperature ($kT_{\rm bb}$) in red and the disc normalisation in blue. Bottom: polarisation degree (Π) in red and polarisation angle (Ψ) in blue. There is no evident correlation of the variability between both. The error bars are shown at 68% confidence levels.

inclination of the system, required by the high polarisation degree, becomes compatible with the maximum inclination expected for the X-ray binaries $i_{\rm max} \sim 78^\circ$ [74]. Whereas the scattering in a completely ionised atmosphere leads to achromatic polarisation degree, absorption processes can lead to its energy dependence [38].

Results from radiative transfer calculations in the approximation of a plane parallel disc atmosphere embedded in flat space-time

In the following we consider the effects of partial ionisation of different atomic species on the polarisation properties using the passive slab of cold matter on top of the unpolarised black-body emission region. This scenario resembles the Milne problem, but the ionisation structure of the medium is pre-computed, rather than parameterised. The radiative transfer calculations account for scattering and absorption effects.

The first model follows the approach discussed by [38, 39]. The calculations use `TITAN` [79] and `CLOUDY` [63] codes to derive one-dimensional vertical ionisation profiles for various photo-ionisation equilibrium (PIE) and collisional

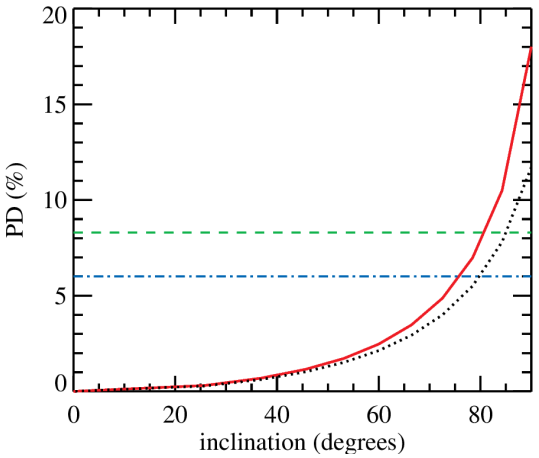

Fig. M4 Polarisation degree as a function of inclination for the pure electron-scattering atmosphere (black dotted), as compared to the case of partial ionisation of matter (absorption effects) and distributed sources (red solid line). The green dashed line indicates the average polarisation in the *IXPE* band and blue dot-dashed line gives the polarisation at about 2 keV.

ionisation equilibrium (CIE) regimes. All of these calculations assume a constant density throughout the atmosphere. As the ionisation profiles from both codes agree with each other, we limit the following discussion to the results obtained with the `TITAN` code. The ionisation profile is subsequently used as input for the 3D Monte Carlo code `STOKES` [80–83], which accounts for line and continuum processes, as well as for multiple scatterings and absorption.

We find that the energy dependent polarisation degree of the emergent emission is governed by the ionisation profiles and depends only weakly on the physical conditions that led to these ionisation profiles. The slab ionisation depends in turn on the density and either on the incident ionisation parameter (in PIE) or on the slab temperature (in CIE). We find that highly ionised slabs can give high polarisation degrees increasing with energy. High ionisation degrees agree with the absence of strong absorption features in the observed energy spectra. Once a sufficiently high ionisation fraction is reached, the polarisation degree saturates and does not change due to a further increase of ionisation for a given slab optical depth, observer's inclination and temperature of the irradiating black-body (if PIE is assumed). Such highly ionised states of the slab are difficult to reach through CIE without any external irradiation, unless extremely high slab temperatures are assumed ($\gtrsim 10^9$ K). However, such temperatures correspond to an inverted temperature profile, with the atmosphere being hotter than the emitting black-body – an unlikely outcome for the optically thick disc atmospheres of X-ray binaries in thermal state [84, 85]. Note that high ionisation represents the most natural state for slabs with hydrogen density $n(\mathrm{H}) \lesssim 10^{20}$ cm^{-3} in PIE, illuminated by black-body radiation at the observed mean X-ray temperatures. Changing the slab density across orders of magnitudes from $n(\mathrm{H}) = 10^{12}$ cm^{-3} to $n(\mathrm{H}) = 10^{20}$ cm^{-3}

does not impact the conclusions. Therefore, the PIE calculations do not constrain the radial dependence of the atmospheric densities. Furthermore, the PIE results are rather insensitive to the ionisation parameter, as long as the slab is highly ionised.

We tested in PIE that the vertical stratification of the atmosphere in up to 50 plane-parallel layers gives the same results as a single layer, as long as the medium is highly ionised. We thus use only one vertically-averaged layer for the following results. We neglect Compton up-scattering, since it would be effective for higher slab temperatures than those considered in our modelling and the effects would be visible at too high energies compared with the *IXPE* band. On the other hand, multiple Compton down-scatterings are included and this process is important in the genesis of polarisation within the *IXPE* band. It was proven that using this approach in the pure-scattering limit we reach the values given by Chandrasekhar's formulae for sufficiently optically thick slabs [38]. We adopted the typical solar abundance from [86] with $A_{\rm Fe} = 1.0$, which is important for the energy-dependent contribution of ionisation edges.

Figure M5 shows the variation of the emergent polarisation degree, plotted as function of energy, with the slab optical depth τ, the observer's inclination and the temperature $kT_{\rm BB}$ of the illuminating black-body in PIE for a highly ionised slab (in a wide energy range). The optical depth is changed only by changing the height of the layer, while the density and the ionisation structure remain constant. In this respect, increasing optical depth and inclination show similar effects, both enhancing the polarisation degree, as the photons are on average reaching the observer through larger portions of the slab. Additional calculations show that vertically stratified atmospheres with BB temperatures down to $kT_{\rm BB} = 0.5$ keV, constant densities up to $n({\rm H}) = 10^{20}$ cm^{-3} and optical thickness $\tau \lesssim 10$ give approximately the same net 2-8 keV polarisation degrees as the simplified approach. The above described model breaks for larger values of optical thickness, since i) the required level of ionisation on the distant (not illuminated) side of the passive slab in PIE is no longer reached, and ii) the assumption of a passive slab is not valid due to the lack of internal sources of X-ray radiation inside the slab. The change of emergent polarisation due to the addition of internal sources is assessed in the next section.

The trend of the polarisation degree with energy shown on Figure M5 can be explained in the following way. From a wider X-ray energy perspective, the cross section for photoelectric absorption declines as $\sim E^{-3}$, while scattering remains roughly constant until ≈ 50 keV and should dominate over absorption already above ≈ 0.2 keV. However, in the *IXPE* band this general trend is reversed; in fact, around 2 keV the photoelectric absorption is insignificant, in accordance with the general trend due to the lack of ionisation edges, while at higher *IXPE* energies the polarisation properties are still strongly affected by absorption (depending on the BB temperature), mostly due to the highly-ionised iron edge. Thus, we are closer to the pure-scattering limit at 2 keV rather than at higher *IXPE* energies. We refer the reader to the detailed study of [84] (figures 1 and 4), which estimates the energy dependent

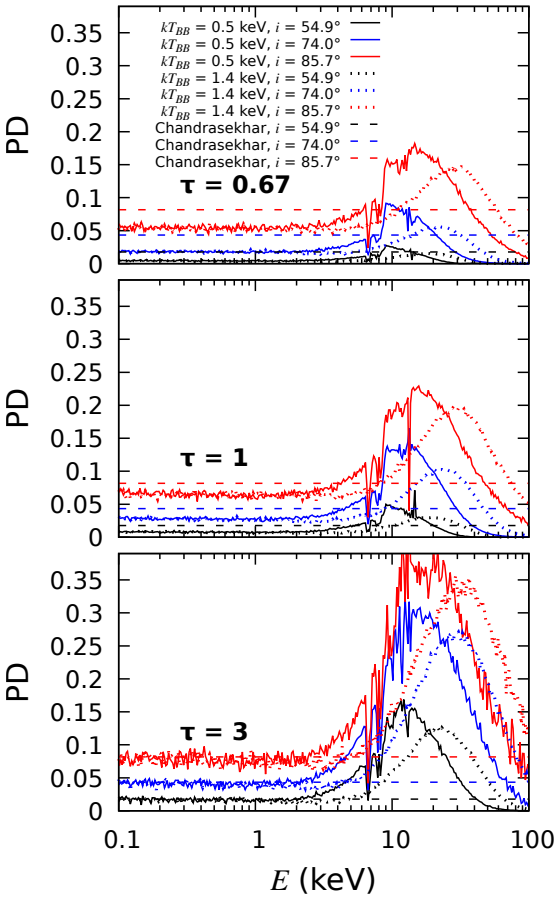

Fig. M5 Polarisation degree vs. energy from the `TITAN` and `STOKES` codes for a highly ionised slab ($n(\mathrm{H}) = 10^{18}$ cm^{-3} and a standard black-body normalisation of the flux at the bottom of the slab). The observer's inclination and optical depth of the slab scale the polarisation degree according to energy dependent contribution of both absorption and scattering. The X-ray black-body temperature of the incident radiation sets weights on different energies. The Chandrasekhar's scattering limit is reached for $\tau \geq 3$ at $E \leq 2$ keV for all significantly contributing single-color black-bodies. The obtained polarisation angle is in all studied cases constant with energy and oriented to be parallel with the slab.

contributions of various processes to the total opacity in the photospheres of BHXRB discs. This is supported by the energy profile of the effective optical depth $\tau_{\mathrm{eff}} \equiv \sqrt{3\tau_{\mathrm{abs}}(\tau_{\mathrm{abs}} + \tau_{\mathrm{es}})}$ [87], where τ_{abs} is the total (sum of bound-free and free-free) absorption optical depth and τ_{es} is the electron scattering optical depth, which can be obtained from the `TITAN` code and which is shown on Figure M6 for our slab computations. The strong ionisation edge seen in the opacities at 9 keV leads to a peak at the same energy in the polarisation degree shown in Figure M5 (and below in Figure M8, using a different model). The absorption effects in polarisation arising from energy dependent opacities are

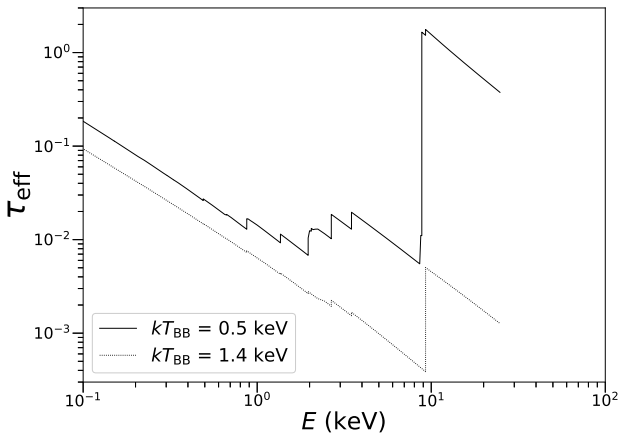

Fig. M6 The effective optical depth vs. energy given by the `TITAN` code for two different irradiating X-ray black-body temperatures from the cases on Figure M5.

further blurred by the energy distribution of the underlying black-body and Compton scattering re-distribution of photons. Our Monte Carlo calculations with `STOKES` predict that absorption has little or no impact on the polarisation degree between 0.2 and 2 keV for $\tau \lesssim 10$, where a plateau in polarisation degree is formed according to the pure-scattering contribution constant with energy. At 2 keV we thus recover Chandrasekhar's result for a pure electron-scattering atmosphere at $\tau \gtrsim 3$ (see Figs. M8 and M9 for the same conclusion at the most significantly contributing disc radii, using a different model assuming a semi-infinite atmosphere and a hydrostatic equilibrium). Thus, the observed 6% polarisation degree at 2 keV robustly constrains the inclination of the emitting patches to be equal or exceed 80° (Figure M4). At the photo-absorption peak around 10 keV, the model allows to raise the emergent polarisation degree. Absorption effects can thus indeed produce a polarisation degree increasing over the *IXPE* energy band, in accordance with the analytical predictions.

Figure M7 shows a fit of the output from these radiative transfer calculations to the *IXPE* data, approximating the accretion disc by a plane parallel slab in flat space. The fitting parameters are the optical depth τ and the inclination i. The best fits are achieved for optically thick slabs ($\tau \approx 5$) and high inclinations ($i \approx 84°$), depending on the single-color BB temperature of the incident radiation. As relativistic effects tend to lower the polarisation degrees, even higher local optical depths and/or inclinations are needed in case of relativistic accretion discs.

Modelling the effects of the impact of radial variations of the properties of the disc photosphere, and relativistic effects

In the next step, we calculate the polarisation of the emission from accretion discs with realistic radially structured disc atmospheres accounting for relativistic effects [88, 89]. In these calculations, the radial disc structure follows

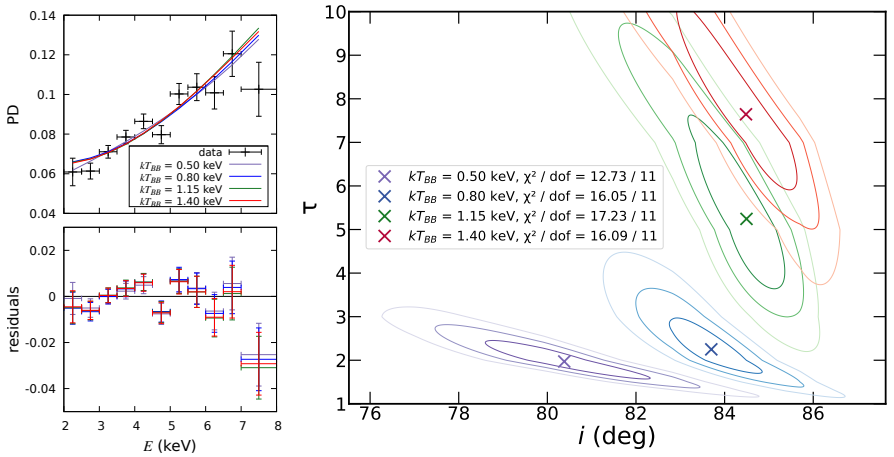

Fig. M7 Best-fit local atmosphere solutions of PD vs. energy (left) and 2D contours of 1σ, 2σ, 3σ levels around their value in i and τ space (right) obtained with `XSPEC` by fitting the energy-dependent data with smoothed `TITAN` and `STOKES` models for $kT_{\rm BB} = 0.5$ keV, $kT_{\rm BB} = 0.8$ keV, $kT_{\rm BB} = 1.15$ keV, $kT_{\rm BB} = 1.4$ keV.

from the conservation laws for mass, angular momentum and energy in accordance with the standard Shakura-Sunyaev α-disc model [9] and the relativistic corrections of [10, 90]. The disc model was divided into a number of rings and the vertical structure of each ring was calculated in the grey approximation using the model atmosphere [91] approach. The model input parameters were taken from the disc parameters at a given radius: effective temperature, half-thickness, and surface density. The ring was assumed to be in hydrostatic and radiative equilibrium. It is also assumed that the local vertical energy release rate is proportional to the local pressure. Then we solve the radiation transfer equation in 0.1 - 20 keV photon energy band in five hundred frequency points using the grey ring model. We use the two-mode approximation, with electron scattering being the only source of polarisation, see details in [92]. We assume no illumination from the top of the atmosphere and a (mirror) reflection boundary condition in the mid-plane of the disc. The plasma equation of state is used assuming local thermodynamic equilibrium. We account for the 15 most abundant chemical elements assuming the solar chemical composition [93]. The ionisation state of the elements and the excited level populations were computed using the Saha-Boltzmann equations including pressure ionisation effects [94]. The absorption opacities were calculated accounting for bound-free and free-free transitions of all the elements. In Figure M8, we present the locally emitted energy spectra for two exemplary rings and five inclinations for $M_{\rm BH} = 10M_{\odot}$, $L = 0.5L_{\rm Edd}$ and $a = 0$. As expected, the polarisation degree exhibits a maximum where the absorption opacity becomes comparable to Thomson scattering.

Exemplary results of the integrated disc spectra are shown in Figure M9. The results are shown before and after accounting for relativistic effects. The

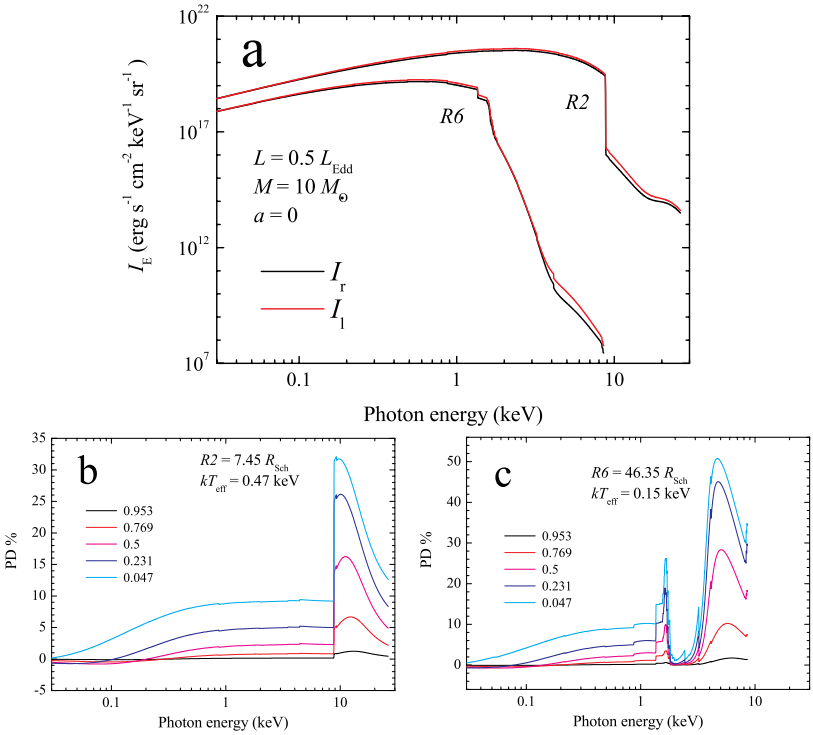

Fig. M8 Spectra of two rings of the considered disc model (see text) in two modes (a), and PD for the same rings (b) and (c). The results in panels (b) and (c) are shown for five angles to the local normal; the cosines of the corresponding angles are shown in the panels.

detailed modelling confirms the results from the simpler models: the polarisation predicted by the standard thin disc model is lower than the observed one. In the next section, we are going to investigate what other effects can help to increase local polarisation degree and compare our models with the observed data.

Comparison of our models with the data

From previous sections it is clear that even if the local polarisation of thermal radiation can be indeed larger than the one estimated by Chandrasekhar approximation [73] if one accounts for the absorption effects, the overall polarisation seen by a distant observer is still too low since the emission is integrated over all disc where relativistic effects – energy shift, light bending, aberration and rotation of polarisation vector along light rays – change the polarisation properties. In this section we would like to compare our model predictions with the observed data in more detail and discuss possible solutions that in principle could still further increase the predicted polarisation degree.

Since the system properties, its inclination and distance, the BH mass and spin, are not measured for this object but rather estimated indirectly, we study

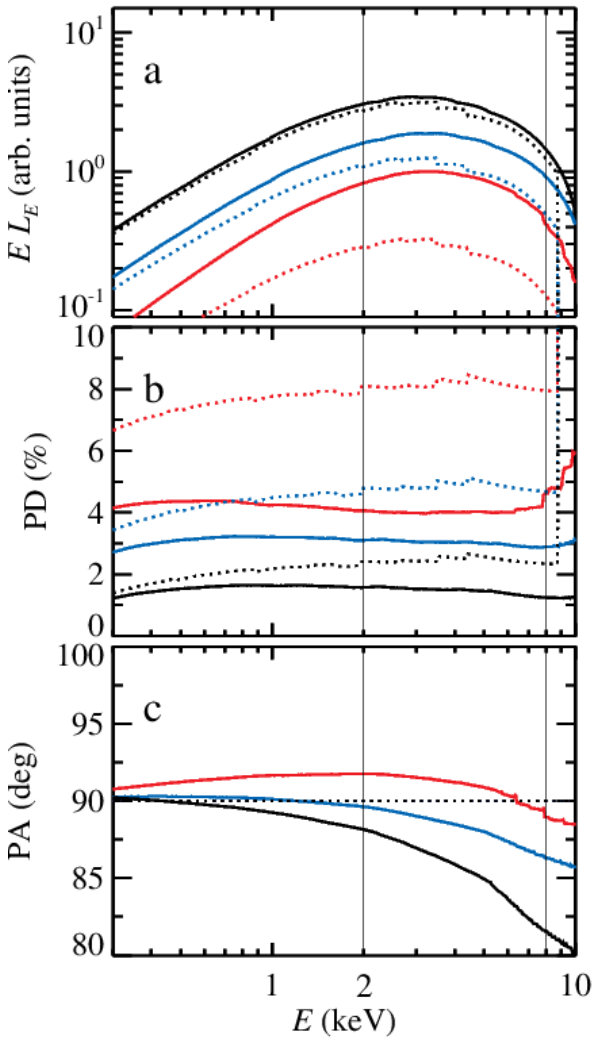

Fig. M9 Spectra, PD and PA from a self-consistent model of the disc atmosphere in radial bins. Dotted lines correspond to quantities in the local reference frame and solid lines correspond to those modified by the relativistic effects, as seen by distant observers. The results are shown for three disc inclinations: $i = 60°$ (black), 75° (blue) and 85° (red).

the polarisation properties of our models assuming several values of rather high inclination and several values of BH spin. The rest of the parameters that change the spectral shape are then fitted from the observed spectrum. Only then we fit the polarisation properties using the observed energy dependence of the polarisation degree and angle to investigate if our model can explain these and whether it can give us any constraints on the spin and/or inclination.

Table M4 The comparison of spectral fit results for different fixed values of system inclination and black hole spin with KYNBBRR model representing the thermal spectral component. If not noted otherwise, a source distance of 11.5 kpc is assumed that corresponds to the normalisation of 0.76. In case the fitted BH mass hit the lower limit of $3\,M_\odot$, we assumed distance of 4.5 kpc corresponding to the model normalisation of 0.49. In case that the fitted BH mass hit the lower limit of $3\,M_\odot$ again, we assumed black hole mass to be $3\,M_\odot$ and fitted the normalisation which corresponds to `norm` $= 1/D_{10}^2$ with D_{10} being the distance to the source in 10 kpc. The fitted values of TBABS and CLOUDY parameters were close to the values shown in Table M2.

Incl.	Spin	Mass	Accretion rate	Normalization	Fit goodness
i (deg)	a	$M_{\rm bh}$ $(M_\odot)$	$\dot{M}/\dot{M}_{\rm Edd}$	norm	χ^2 (792 dof)
70	0	3 (frozen)	0.451 ± 0.003	2.13 ± 0.02 [a]	730
	0.998	23.59 ± 0.10	0.1221 ± 0.0003	0.75614 (frozen)	638
75	0	3 (frozen)	0.424 ± 0.003	3.02 ± 0.03 [b]	719
	0.5	3.59 ± 0.02	0.1992 ± 0.0005	4.93827 (frozen)	732
	0.7	3.80 ± 0.02	0.1759 ± 0.0005	4.93827 (frozen)	719
	0.9	15.57 ± 0.07	0.2402 ± 0.0006	0.75614 (frozen)	670
	0.998	29.5 ± 0.1	0.1005 ± 0.0002	0.75614 (frozen)	632
85	0	3 (frozen)	0.6336 ± 0.0005	4.93827 (frozen)	728
	0.998	48.7 ± 0.2	0.0724 ± 0.0002	0.75614 (frozen)	629

[a] corresponding to the distance of 6.85 kpc

[b] corresponding to the distance of 5.75 kpc

For our spectral fit we use only the *NICER* data set since only the *NICER* observation covers the *IXPE* one well enough throughout the whole observation. We take *NICER* data corresponding to *IXPE* observing period and sum them together using `addspec` tool from the `HEASOFT` package [55]. The *NuSTAR* data cover only a small fraction of *IXPE* observation thus we just use it to estimate the contribution of non-thermal component to the total observed flux. Since the spectra observed by *NICER* are much better calibrated, especially for high flux sources, compared to the spectra observed by *IXPE*, we use only the polarisation data from *IXPE*.

From the three *NuSTAR* observations we see that the non-thermal component is highly variable and contributing only by few percent in the 2–8 keV energy band. Therefore in the following analysis we use only an absorbed thermal component. To fit the *NICER* spectra, we use the model EDGE×TBABS×CLOUDY(KYNBBRR). Here, we use the Novikov-Thorne geometrically thin disc model KYNBBRR [35, 38, 95] instead of and similar to KERRBB model for the thermal component since this model allows us to study also the polarisation properties of this component in different scenarios. The other model components are the same as already described in the spectral analysis section. We emphasise that in the current analysis we use the summed *NICER* data, i.e. not only the data correspondent to *NuSTAR* observations, we exclude non-thermal component and we fit for several assumed values of inclinations and BH spins, contrary to what we have done in the spectral analysis section. In the current spectral analysis we use 1% systematic error for the *NICER* data. Note that the spectral fit does not require the Comptonised component at these energies confirming that its average contribution is very low in the

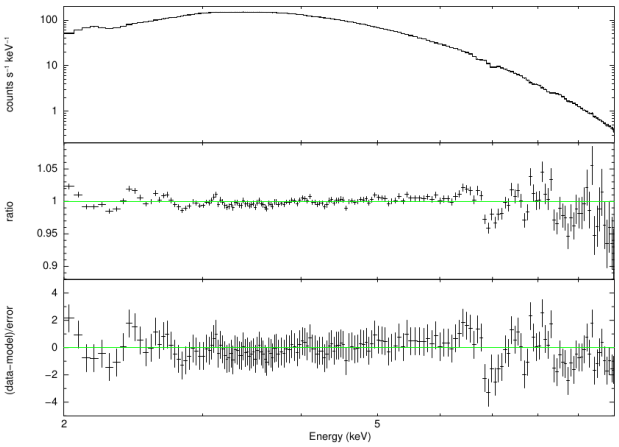

Fig. M10 Example of the best fit model to the *NICER* data (top), ratio of data to the fitted model (middle) and the data residuals from the model (bottom) for the case with assumed inclination $\theta = 75°$ and BH spin $a = 0.5$. Other studied cases give fits of similar quality.

full *IXPE* observation. The best spectral fits are summarised in the Table M4 and one example fit (inclination $\theta = 75°$ and BH spin $a = 0.5$) is shown on Figure M10.

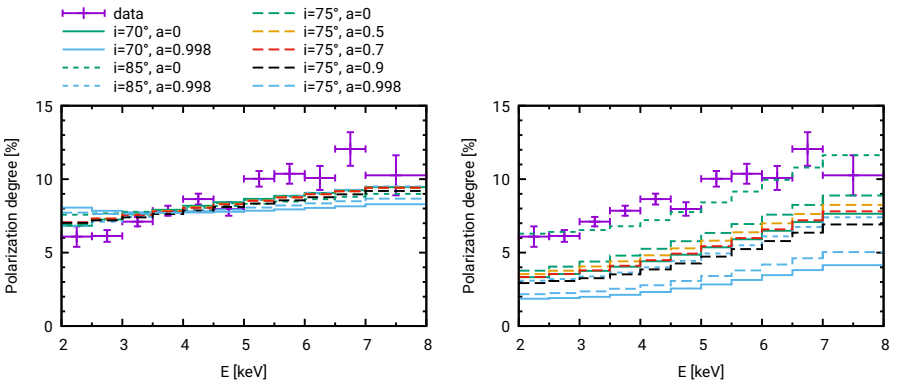

Fig. M11 Attempted fits of observed polarisation degree with the models (B) (left) and (C) (right). See the text for details. We did not account for self-irradiation in these computations.

In the next step we freeze all the parameters influencing the spectral shape and try to fit the polarisation degree and angle observed by *IXPE* and reduced as described in the data reduction section. To this purpose, we have developed different flavours of the KYNBBRR polarisation model that originally assumed Chandrasekhar approximation of pure scattering atmosphere for direct radiation and Chandrasekhar multi-scattering approximation for polarisation of reflected disc self-irradiation with an assumed albedo of 0.5. We denote this original model as model (A). The orientation of the system on the sky of the

Table M5 Comparison of goodness of polarisation degree and angle fits using different flavours of the KYNBBRR model. Note that both the PD and PA was binned in 11 energy bins. The fits with $\chi^2_{\rm tot} < 22$ are denoted in bold and the best fit parameter values of these cases are shown in Table M6.

Incl.	Spin	model (A)	model (B)	model (C)	model (D)
i (deg)	a	χ^2(PD/PA/tot)	χ^2(PD/PA/tot)	χ^2(PD/PA/tot)	χ^2(PD/PA/tot)
70	0	1573/8.9/1581	33/8.0/40	626/7.7/634	**11.5/7.9/19.4**
	0.998	2236/280/2517	84/80/164	1551/66/1617	12.2/57/69
75	0	1132/7.8/1140	35/7.8/43	387/7.7/395	**11.8/7.8/19.6**
	0.5	1529/13/1542	37/8.8/45	506/8.3/514	**12.2/8.3/20.5**
	0.7	1722/21/1743	37/10/47	606/9.8/616	**12.5/9.3/21.8**
	0.9	2077/53/2130	41/15/56	828/15/843	12.7/12.9/25.7
	0.998	2162/258/2420	65/56/121	1309/48/1357	12.1/41/53
85	0	658/7.8/666	55/7.7/63	42/7.9/50	**13.3/7.9/21.2**
	0.998	2098/187/2285	30/21/51	765/21/786	12.9/18.6/31.54

Table M6 The best fit parameters of the KYNBBRR model (D) with outflowing ionised layer. Since the optical thickness of the layer and its outflow speed were degenerate, we eventually kept optical thickness to be frozen to $\tau = 7$. We characterise the outflow speed by its value at the radius where the disc temperature peaks, $\beta(T_{\rm max})$, see the last column.

Incl.	Spin	orientation	speed norm	speed index	speed
i (deg)	a	$\chi_{\rm o}$	β_0	q	$\beta(T_{\rm max})$
70	0	-70.7 ± 0.5	0.65 ± 0.14	0.54 ± 0.19	0.50
75	0	-71.2 ± 0.5	0.56 ± 0.18	0.72 ± 0.29	0.40
	0.5	-70.1 ± 0.5	0.65 ± 0.18	0.73 ± 0.26	0.47
	0.7	-68.9 ± 0.5	0.71 ± 0.17	0.70 ± 0.23	0.53
85	0	-72.5 ± 0.5	0.6 (frozen)	2.1 ± 0.2	0.22

observer is the only free parameter of this model to fit the observed polarisation properties. It defines the direction of the system rotation axis. As mentioned in the previous section, the predicted polarisation degree of this model is too low, see the left panel on Figure 2 and Table M5. To increase the local polarisation degree in this model, one would have to assume larger emission angle in local reference frame co-moving with the accretion disc. This could happen in case of an outflow with relativistic speeds in the vertical direction, i.e. perpendicular to the disc. Due to relativistic aberration effect, the photons would then need to be emitted with higher emission angles to reach the same observer at a given inclination angle. Thus in the second flavour of this polarisation model, denoted as (B), we assume decreasing radial profile of the vertical outflow velocity, i.e. $\beta(r) = \beta_0\, r^{-q}$ with β being the speed in units of speed of light in the vacuum. This model then has two new parameters, β_0 and q, that influence the predicted polarisation properties. This model still does not fit the observed polarisation very well, see the left panel on Figure M11 and Table M5. While the model reaches high values of polarisation degree it fails to fit its increase with energy. The third flavour of the polarisation model, denoted here as (C), uses the local polarisation degree defined by the local model from previous sections (the one for an ionized passive slab with finite optical depth and constant density computed with the `TITAN` and `STOKES` codes). The local

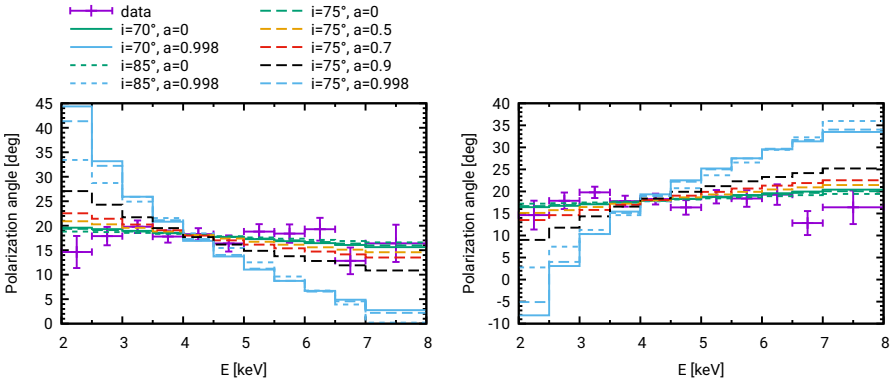

Fig. M12 Polarisation angle predicted by the model (A). Note, however, that the PA energy dependence predicted with different flavours of the KYNBBRR model is very similar due to the fact that the local polarisation angle is always assumed to be parallel with the disc. The predicted PA is thus dependent mainly on the relativistic effects. The PA for both anticlock-wise (left) and clock-wise (right) direction of the system rotation are shown (the disc and black hole are co-rotating in both cases).

polarisation degree in this model depends on the disc temperature (given by the Novikov-Thorne temperature profile), emission angle (computed by ray-tracing in the curved space-time for a given observer inclination) and optical thickness of this layer. The last parameter is then a new parameter that influences the predicted polarisation properties of this model. As mentioned in the previous sections, this model also does not fit the observed polarisation properties, see the right panel on Figure M11 and Table M5. Although the increase of polarisation degree with energy is corresponding to the observed increase, the magnitude of the polarisation degree is too low. To increase the predicted polarisation degree of this model, we increase the local polarisation degree by assuming vertical outflow velocity that causes higher local emission angle due to aberration effect as in model (B). We denote this model as model (D). The top right panel on Figure 2 and Table M5 shows that this model can fit the observed data quite well except for highly spinning black holes that do not fit the observed polarisation angle, see Figure M12. Acceptable fits are denoted by bold-face in Table M5 and the best fit parameters are shown in Table M6. Note that to achieve the observed polarisation degree the scattering layer has to be outflowing with approximately half of light speed.

Up to now we have investigated possibilities how to increase the polarisation degree in our model of thermal emission that is seen directly by the observer. Another way how to increase the total polarisation degree of the thermal component would be by increasing the contribution of polarised flux due to reflection of the disc self-irradiation. This flux is already quite highly polarised thus the reflected flux itself would have to be increased. Since this is dependent on the amount of self-irradiation, this can be larger only if we change the disc geometry, specifically if the disc scale height will be substantially larger than in the geometrically thin accretion disc, where it is usually

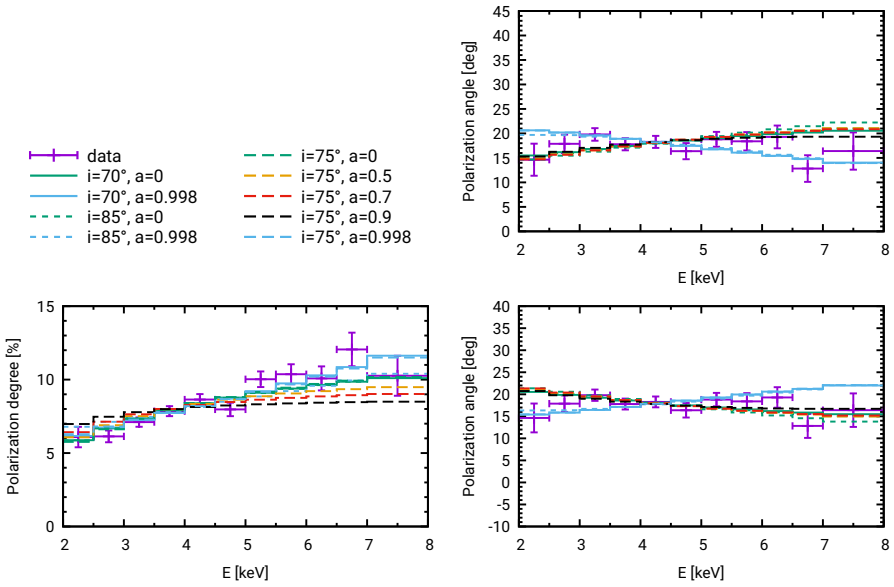

Fig. M13 The polarisation degree (left) and polarisation angle energy dependence for anticlock-wise (top right) and clock-wise (bottom right) direction of the system rotation for geometrically thin disc with the contribution of the reflected self-irradiation increased by allowing the albedo to be larger than 1.

assumed that, $h/r \ll 1$ for the scale height h of the disc at radius r. This possibility is investigated in more detail in the next section. For a rough estimate of how much the self-irradiation would need to be increased, we can use the geometrically thin disc scenario where the albedo will be allowed to be larger than one. The results of this experiment is shown on Figure M13. While the exact shape of the model predicted polarisation degree and angle and thus also the dependence of the fit statistics on model parameters should be taken with care, since the model is not self-consistent any more, we can still discuss the value of the albedo and its interpretation with respect to amount of self-irradiation. The albedo is the lowest for the highest studied spin value and increases for lower spin values while it depends much less on the inclination. This is due to the fact that the amount of self-irradiation is already much larger in case of the disc reaching closer to the black hole horizon for highly spinning BH thus smaller multiplicative factor (albedo) is needed to reach the needed increase in polarised reflected flux. On the other hand the amount of the reflected self-irradiation depends much less on the inclination. For the inclination of 75°, the fitted albedo value was 4.5, 11.4, 17.1, 22.2 and 36.2 for the spin values of 0.998, 0.9, 0.7, 0.5 and 0, respectively. Thus for highly ionised discs, where the physical value of the albedo is expected to be between 0.5 and 1, we would need the self-irradiated flux to increase by a factor of 5 to 10 in case of very highly spinning BH.

Polarisation of the emission from slim and thick accretion discs

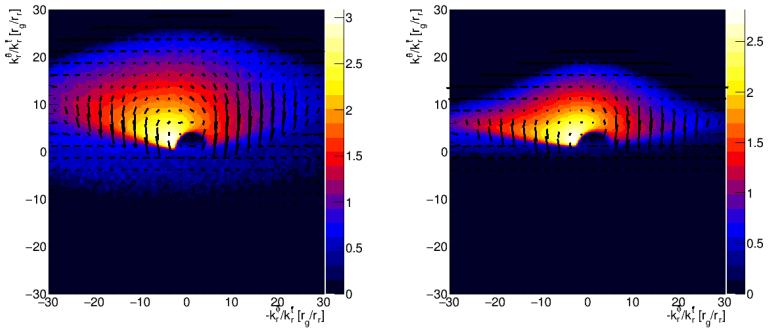

Fig. M14 Total flux for ray-traced simulations of 0.98 spin black holes with $h/r = 0.5$ viewed at a 75° inclination (left) and $h/r = 0.3$ viewed at an 85° inclination (right). The colour scale shows the flux on a logarithmic scale in arbitrary units. Overlaid, the black vectors indicate the PA and have a length proportional to the PD – both as seen by a distant observer.

We also explored if the polarisation of X-rays from phenomenological thick disc models [96] could explain the *IXPE* data. The models assume discs of various scale heights embedded in the Kerr space-time. The disc matter is assumed to orbit the black hole on general relativistic Keplerian orbits. Following the classical treatment of [97], it is assumed that the disc material locally emits all the net energy that it gains by sinking towards the black hole. Given the energy liberated in each radial bin per co-moving time, the temperature of the disc surface is calculated from the Stefan-Boltzmann law accounting for the fact that a thicker disc has a larger surface area than a geometrically thin disc. It is furthermore assumed that the disc emits locally a modified black-body energy spectrum adopting a constant spectral hardening factor of 1.8. The surface of the disc follows a simple phenomenological description inspired by the Polish doughnut models by [13]. The discs are characterised by the scale height, h/r with h being the height of the disc where the disc is thickest, and r being the corresponding disc radius.

Figure M14 shows the 2-D distribution of the surface brightness, PD, and PA, as a distant observer would see them. Both models show the effect of the colder and X-ray dimmer outer portions of the slim discs shadowing the emission from the hot and bright inner regions. Figure M15 shows the PD and PA energy spectra for discs scale heights ranging between 0 and 0.9. The PDs always increase with energy, as the highest-energy emission from the innermost portion of the disc are most likely to scatter off the opposite side of the disc. The PAs stay roughly constant with energy.

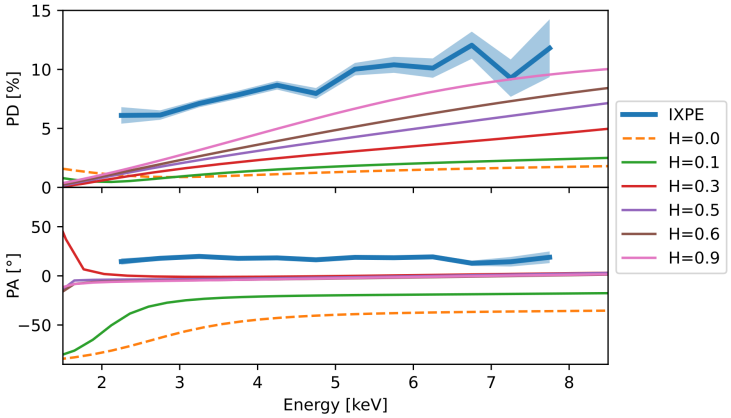

Fig. M15 Polarisation degrees (top) and angles (bottom) for thin, slim, and thick discs of 0.98 spin viewed at $i = 85°$, assuming a highly-ionised disc photosphere. The model predictions are marked by solid lines of different colours, while *IXPE* data are reported as a blue line in both panels. The shaded cyan region represents the errors at 68% confidence level. Note that while the PA is unknown still its behaviour with energy is constrained to be consistent with a constant. Almost all our studied slim and thick geometries fullfil this except those with very low scaleheight and high BH spin.

The figure shows that increasing scale heights lead to overall higher PDs. We could, however, not find a parameter combination that achieves polarisation degrees as high as the observed ones.

Figure M16 shows that the PDs increase with inclination and with the black hole spin. The dependence of the PD on inclination results from the combined effects of different inclinations of the emission reaching the observer, and different degrees of self-shadowing of the emission by thick discs. Increasing black hole spins lead to higher PDs as higher spins correspond to the discs extending closer to the black holes, and leading to a higher fractions of photons reflecting off the discs.

Acknowledgements

The *IXPE* is a joint US and Italian mission. The US contribution is supported by NASA and led and managed by its Marshall Space Flight Center (MSFC), with industry partner Ball Aerospace (contract no. NNM15AA18C). The Italian contribution is supported by the Italian Space Agency (Agenzia Spaziale Italiana, ASI) through contract no. ASI-OHBI-2017-12-I.0, agreement nos. ASI-INAF-2017-12-H0 and ASI-INFN-2017.13-H0, and its Space Science Data Center (SSDC) with agreement nos. ASI-INAF-2022-14-HH.0 and ASI-INFN 2021-43-HH.0, and by the Istituto Nazionale di Astrofisica (INAF) and the Istituto Nazionale di Fisica Nucleare (INFN) in Italy. This research used data products provided by the *IXPE* Team (MSFC, SSDC,

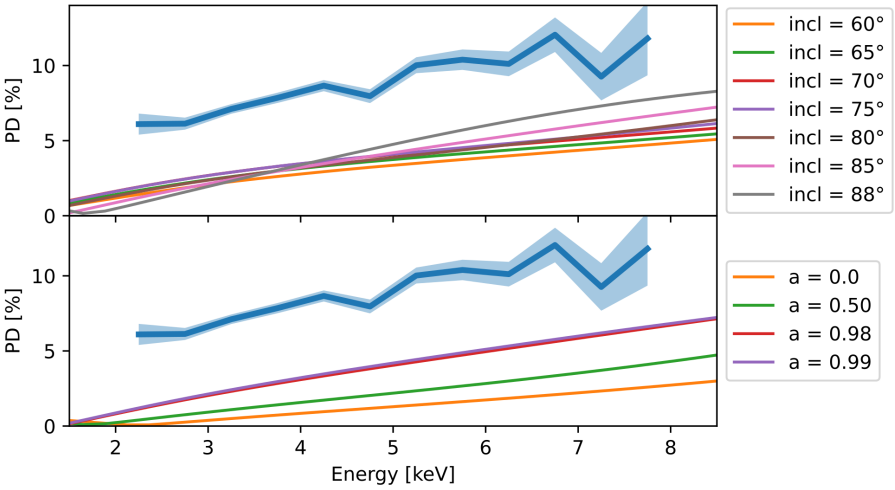

Fig. M16 Polarisation degree predictions of 0.5 scale height discs. Top panel: Results for a black hole with 0.99 spin viewed at different inclination angles. Bottom panel: Results for a black hole at 85° with varying spins.

INAF and INFN) and distributed with additional software tools by the High-Energy Astrophysics Science Archive Research Center (HEASARC), at NASA Goddard Space Flight Center (GSFC). A.R. and F.T. thank Prof. Keigo Fukumura for useful discussions. M.D., J.Pod., J.S. and V.K. acknowledge the support from the Czech Science Foundation project GACR 21-06825X and the institutional support from the Astronomical Institute of the Czech Academy of Sciences RVO:67985815. J.Pod. and V.K. thank the Czech-Polish mobility program (MŠMT 8J20PL037 and PPN/BCZ/2019/1/00069) and the European Space Agency PRODEX project 4000132152. M.D. and J.Pod. specially thank Prof. Agata Różańska for explanations and guidance using the `TITAN` code. H.K., N.R.C. and A.W. acknowledge NASA support through the grants NNX16AC42G, 80NSSC20K0329, 80NSSC20K0540, NAS8-03060, 80NSSC21K1817, 80NSSC22K1291, and 80NSSC22K1883 as well as support from the McDonnell Center for the Space Sciences. V.S. acknowledge Deutsche Forschungsgemeinschaft (DFG) support through the grant WE 1312/59-1 and the German Academic Exchange Service (DAAD) support through the project 57525212. A.I. acknowledges support from the Royal Society. The french contribution acknowledges financial support from the french High Energy national program from CNRS and from the french spatial agency (CNES). M.N. acknowledges the support by NASA under award number 80GSFC21M0002.

Data availability

The *IXPE*, *NICER* and *NuSTAR* data used in this analysis are from the HEASARC data archive.

Competing Interests Statement

Authors declare no competing interests.

Contributions

A.R., M.D., H.K., J.Pod., L.M., A.V., V.S., N.R.C., J.St., J.Sv., A.Ma., S.B., M.N. and F.C. participated in the planning of the observation campaign and the analysis and modeling of the data. G.M., F.T., J.Pou., A.I., R.T., A.W. contributed to the analysis or modeling of the data. F.U. and V.K. served as internal referees. P.S., D.V., A.Man., F.M., M.P., B.B., S.C., N.C., N.D.L., S.F., K.H., P.K., V.L., R.M., T.M., N.O., P.-O.P., S.P., J.R., S.Za., S.Zh. contributed to the discussion of the results. All other authors contributed to the design and science case of the IXPE mission and to planning the observations used in this paper. All authors provided input and comments on the manuscript.

References

[1] Ponti, G., Fender, R.P., Begelman, M.C., Dunn, R.J.H., Neilsen, J., Coriat, M.: Ubiquitous equatorial accretion disc winds in black hole soft states. MNRAS **422**(1), 11–15 (2012) arXiv:1201.4172 [astro-ph.HE]. https://doi.org/10.1111/j.1745-3933.2012.01224.x

[2] Mészáros, P., Rees, M.J.: Poynting Jets from Black Holes and Cosmological Gamma-Ray Bursts. Astrophys. Lett. **482**(1), 29–32 (1997) arXiv:astro-ph/9609065 [astro-ph]. https://doi.org/10.1086/310692

[3] Fender, R.P.: Powerful jets from black hole X-ray binaries in low/hard X-ray states. MNRAS **322**(1), 31–42 (2001) arXiv:astro-ph/0008447 [astro-ph]. https://doi.org/10.1046/j.1365-8711.2001.04080.x

[4] Weisskopf, M.C., Soffitta, P., Baldini, L., Ramsey, B.D., O'Dell, S.L., Romani, R.W., Matt, G., Deininger, W.D., Baumgartner, W.H., Bellazzini, R., Costa, E., Kolodziejczak, J.J., Latronico, L., Marshall, H.L., Muleri, F., Bongiorno, S.D., Tennant, A., Bucciantini, N., Dovciak, M., Marin, F., Marscher, A., Poutanen, J., Slane, P., Turolla, R., Kalinowski, W., Di Marco, A., Fabiani, S., Minuti, M., La Monaca, F., Pinchera, M., Rankin, J., Sgro', C., Trois, A., Xie, F., Alexander, C., Allen, D.Z., Amici, F., Andersen, J., Antonelli, A., Antoniak, S., Attinà, P., Barbanera, M., Bachetti, M., Baggett, R.M., Bladt, J., Brez, A., Bonino, R., Boree, C., Borotto, F., Breeding, S., Brienza, D., Bygott, H.K., Caporale, C., Cardelli, C., Carpentiero, R., Castellano, S., Castronuovo, M., Cavalli, L., Cavazzuti, E., Ceccanti, M., Centrone, M., Citraro, S., D'Amico, F., D'Alba, E., Di Gesu, L., Del Monte, E., Dietz, K.L., Di Lalla, N., Persio, G.D., Dolan, D., Donnarumma, I., Evangelista, Y., Ferrant, K.,

Ferrazzoli, R., Ferrie, M., Footdale, J., Forsyth, B., Foster, M., Garelick, B., Gunji, S., Gurnee, E., Head, M., Hibbard, G., Johnson, S., Kelly, E., Kilaru, K., Lefevre, C., Roy, S.L., Loffredo, P., Lorenzi, P., Lucchesi, L., Maddox, T., Magazzu, G., Maldera, S., Manfreda, A., Mangraviti, E., Marengo, M., Marrocchesi, A., Massaro, F., Mauger, D., McCracken, J., McEachen, M., Mize, R., Mereu, P., Mitchell, S., Mitsuishi, I., Morbidini, A., Mosti, F., Nasimi, H., Negri, B., Negro, M., Nguyen, T., Nitschke, I., Nuti, A., Onizuka, M., Oppedisano, C., Orsini, L., Osborne, D., Pacheco, R., Paggi, A., Painter, W., Pavelitz, S.D., Pentz, C., Piazzolla, R., Perri, M., Pesce-Rollins, M., Peterson, C., Pilia, M., Profeti, A., Puccetti, S., Ranganathan, J., Ratheesh, A., Reedy, L., Root, N., Rubini, A., Ruswick, S., Sanchez, J., Sarra, P., Santoli, F., Scalise, E., Sciortino, A., Schroeder, C., Seek, T., Sosdian, K., Spandre, G., Speegle, C.O., Tamagawa, T., Tardiola, M., Tobia, A., Thomas, N.E., Valerie, R., Vimercati, M., Walden, A.L., Weddendorf, B., Wedmore, J., Welch, D., Zanetti, D., Zanetti, F.: The Imaging X-Ray Polarimetry Explorer (IXPE): Pre-Launch. Journal of Astronomical Telescopes, Instruments, and Systems **8**(2), 026002 (2022) arXiv:2112.01269 [astro-ph.IM]. https://doi.org/10.1117/1.JATIS.8.2.026002

[5] Krawczynski, H., Beheshtipour, B.: New Constraints on the Spin of the Black Hole Cygnus X-1 and the Physical Properties of its Accretion Disk Corona. ApJ **934**(1), 4 (2022) arXiv:2201.07360 [astro-ph.HE]. https://doi.org/10.3847/1538-4357/ac7725

[6] Remillard, R.A., McClintock, J.E.: X-Ray Properties of Black-Hole Binaries. ARA&A **44**(1), 49–92 (2006) arXiv:astro-ph/0606352 [astro-ph]. https://doi.org/10.1146/annurev.astro.44.051905.092532

[7] Done, C., Gierliński, M., Kubota, A.: Modelling the behaviour of accretion flows in X-ray binaries. Everything you always wanted to know about accretion but were afraid to ask. A&ARv **15**(1), 1–66 (2007) arXiv:0708.0148 [astro-ph]. https://doi.org/10.1007/s00159-007-0006-1

[8] Veledina, A., Muleri, F., Poutanen, J., Podgorný, J., Dovčiak, M., Capitanio, F., Churazov, E., De Rosa, A., Di Marco, A., Forsblom, S., Kaaret, P., Krawczynski, H., La Monaca, F., Loktev, V., Lutovinov, A.A., Molkov, S.V., Mushtukov, A.A., Ratheesh, A., Rodriguez Cavero, N., Steiner, J.F., Sunyaev, R.A., Tsygankov, S.S., Zdziarski, A.A., Bianchi, S., Bright, J.S., Bursov, N., Costa, E., Egron, E., Garcia, J.A., Green, D.A., Gurwell, M., Ingram, A., Kajava, J.J.E., Kale, R., Kraus, A., Malyshev, D., Marin, F., Matt, G., McCollough, M., Mereminskiy, I.A., Nizhelsky, N., Piano, G., Pilia, M., Pittori, C., Rao, R., Righini, S., Soffitta, P., Shevchenko, A., Svoboda, J., Tombesi, F., Trushkin, S., Tsybulev, P., Ursini, F., Weisskopf, M.C., Wu, K., Agudo, I., Antonelli, L.A., Bachetti, M., Baldini, L., Baumgartner, W.H., Bellazzini, R., Bongiorno, S.D., Bonino, R., Brez, A.,

Bucciantini, N., Castellano, S., Cavazzuti, E., Chen, C.-T., Ciprini, S., Del Monte, E., Di Gesu, L., Di Lalla, N., Donnarumma, I., Doroshenko, V., Ehlert, S.R., Enoto, T., Evangelista, Y., Fabiani, S., Ferrazzoli, R., Gunji, S., Hayashida, K., Heyl, J., Iwakiri, W., Jorstad, S.G., Karas, V., Kislat, F., Kitaguchi, T., Kolodziejczak, J.J., Latronico, L., Liodakis, I., Maldera, S., Manfreda, A., Marinucci, A., Marscher, A.P., Marshall, H.L., Massaro, F., Mitsuishi, I., Mizuno, T., Negro, M., Ng, C.-Y., O'Dell, S.L., Omodei, N., Oppedisano, C., Papitto, A., Pavlov, G.G., Peirson, A.L., Perri, M., Pesce-Rollins, M., Petrucci, P.-O., Possenti, A., Puccetti, S., Ramsey, B.D., Rankin, J., Roberts, O., Romani, R.W., Sgrò, C., Slane, P., Spandre, G., Swartz, D., Tamagawa, T., Tavecchio, F., Taverna, R., Tawara, Y., Tennant, A.F., Thomas, N.E., Trois, A., Turolla, R., Vink, J., Xie, F., Zane, S.: Astronomical puzzle Cyg X-3 is a hidden Galactic ultraluminous X-ray source. arXiv e-prints, 2303–01174 (2023) arXiv:2303.01174 [astro-ph.HE]. https://doi.org/10.48550/arXiv.2303.01174

[9] Shakura, N.I., Sunyaev, R.A.: Black holes in binary systems. Observational appearance. A&A **24**, 337–355 (1973)

[10] Novikov, I.D., Thorne, K.S.: Astrophysics of black holes. In: Black Holes (Les Astres Occlus), pp. 343–450 (1973)

[11] Esin, A.A., McClintock, J.E., Narayan, R.: Advection-Dominated Accretion and the Spectral States of Black Hole X-Ray Binaries: Application to Nova Muscae 1991. ApJ **489**(2), 865–889 (1997) arXiv:astro-ph/9705237 [astro-ph]. https://doi.org/10.1086/304829

[12] McClintock, J.E., Remillard, R.A.: Black Hole Binaries. arXiv (2003). https://doi.org/10.48550/ARXIV.ASTRO-PH/0306213. https://arxiv.org/abs/astro-ph/0306213

[13] Abramowicz, M.A., Czerny, B., Lasota, J.P., Szuszkiewicz, E.: Slim Accretion Disks. ApJ **332**, 646 (1988). https://doi.org/10.1086/166683

[14] Giacconi, R., Murray, S., Gursky, H., Kellogg, E., Schreier, E., Tananbaum, H.: The Uhuru catalog of X-ray sources. ApJ **178**, 281–308 (1972). https://doi.org/10.1086/151790

[15] Priedhorsky, W.: Recurrent Population II X-ray transients — similarities to SU UMa cataclysmic variables. Ap&SS **126**(1), 89–98 (1986). https://doi.org/10.1007/BF00644177

[16] Kuulkers, E., Wijnands, R., Belloni, T., Méndez, M., van der Klis, M., van Paradijs, J.: Absorption Dips in the Light Curves of GRO J1655-40 and 4U 1630-47 during Outburst. ApJ **494**(2), 753–758 (1998) arXiv:astro-ph/9710024 [astro-ph]. https://doi.org/10.1086/305248

[17] Capitanio, F., Campana, R., De Cesare, G., Ferrigno, C.: Missing hard states and regular outbursts: the puzzling case of the black hole candidate 4U 1630-472. MNRAS **450**(4), 3840–3854 (2015) arXiv:1505.04034 [astro-ph.HE]. https://doi.org/10.1093/mnras/stv687

[18] Reid, C.A., Johnston, M.D., Bradt, H.V., Doxsey, R.E., Griffiths, R.E., Schwartz, D.A.: Unidentified galactic X-ray sources positioned with the HEAO-1 scanning modulation collimator. AJ **85**, 1062–1070 (1980). https://doi.org/10.1086/112768

[19] Parmar, A.N., Stella, L., White, N.E.: The Evolution of the 1984 Outburst of the Transient X-Ray Source 4U 1630-47. ApJ **304**, 664 (1986). https://doi.org/10.1086/164204

[20] Kalemci, E., Maccarone, T.J., Tomsick, J.A.: A Dust-scattering Halo of 4U 1630-47 Observed with Chandra and Swift: New Constraints on the Source Distance. ApJ **859**(2), 88 (2018) arXiv:1804.02909 [astro-ph.HE]. https://doi.org/10.3847/1538-4357/aabcd3

[21] Tomsick, J.A., Lapshov, I., Kaaret, P.: An X-Ray Dip in the X-Ray Transient 4U 1630-47. ApJ **494**(2), 747–752 (1998) arXiv:astro-ph/9709214 [astro-ph]. https://doi.org/10.1086/305240

[22] Díaz Trigo, M., Migliari, S., Miller-Jones, J.C.A., Guainazzi, M.: XMM-Newton observations reveal the disappearance of the wind in 4U 1630-47. A&A **571**, 76 (2014) arXiv:1409.3406 [astro-ph.HE]. https://doi.org/10.1051/0004-6361/201424554

[23] King, A.L., Walton, D.J., Miller, J.M., Barret, D., Boggs, S.E., Christensen, F.E., Craig, W.W., Fabian, A.C., Fürst, F., Hailey, C.J., Harrison, F.A., Krivonos, R., Mori, K., Natalucci, L., Stern, D., Tomsick, J.A., Zhang, W.W.: The Disk Wind in the Rapidly Spinning Stellar-mass Black Hole 4U 1630-472 Observed with NuSTAR. Astrophys. Lett. **784**(1), 2 (2014) arXiv:1401.3646 [astro-ph.HE]. https://doi.org/10.1088/2041-8205/784/1/L2

[24] Miller, J.M., Fabian, A.C., Kaastra, J., Kallman, T., King, A.L., Proga, D., Raymond, J., Reynolds, C.S.: Powerful, Rotating Disk Winds from Stellar-mass Black Holes. ApJ **814**(2), 87 (2015) arXiv:1510.01177 [astro-ph.HE]. https://doi.org/10.1088/0004-637X/814/2/87

[25] Tomsick, J.A., Corbel, S., Goldwurm, A., Kaaret, P.: X-Ray Observations of the Black Hole Transient 4U 1630-47 during 2 Years of X-Ray Activity. ApJ **630**(1), 413–429 (2005) arXiv:astro-ph/0505271 [astro-ph]. https://doi.org/10.1086/431896

[26] Baldini, L., Bucciantini, N., Lalla, N.D., Ehlert, S., Manfreda, A., Negro,

M., Omodei, N., Pesce-Rollins, M., Sgrò, C., Silvestri, S.: ixpeobssim: A simulation and analysis framework for the imaging X-ray polarimetry explorer. SoftwareX **19**, 101194 (2022) arXiv:2203.06384 [astro-ph.IM]. https://doi.org/10.1016/j.softx.2022.101194

[27] Matsuoka, M., Kawasaki, K., Ueno, S., Tomida, H., Kohama, M., Suzuki, M., Adachi, Y., Ishikawa, M., Mihara, T., Sugizaki, M., Isobe, N., Nakagawa, Y., Tsunemi, H., Miyata, E., Kawai, N., Kataoka, J., Morii, M., Yoshida, A., Negoro, H., Nakajima, M., Ueda, Y., Chujo, H., Yamaoka, K., Yamazaki, O., Nakahira, S., You, T., Ishiwata, R., Miyoshi, S., Eguchi, S., Hiroi, K., Katayama, H., Ebisawa, K.: The MAXI Mission on the ISS: Science and Instruments for Monitoring All-Sky X-Ray Images. PASJ **61**, 999 (2009) arXiv:0906.0631 [astro-ph.IM]. https://doi.org/10.1093/pasj/61.5.999

[28] Jiang, J., Tomsick, J., Liu, H., Fabian, A., Connors, R., Garcia, J., Hare, J.: Swift Follow-up of 4U 1630-47 in Outburst. The Astronomer's Telegram **15575**, 1 (2022)

[29] Arzoumanian, Z., Gendreau, K.C., Baker, C.L., Cazeau, T., Hestnes, P., Kellogg, J.W., Kenyon, S.J., Kozon, R.P., Liu, K.-C., Manthripragada, S.S., Markwardt, C.B., Mitchell, A.L., Mitchell, J.W., Monroe, C.A., Okajima, T., Pollard, S.E., Powers, D.F., Savadkin, B.J., Winternitz, L.B., Chen, P.T., Wright, M.R., Foster, R., Prigozhin, G., Remillard, R., Doty, J.: The neutron star interior composition explorer (NICER): mission definition. In: Takahashi, T., den Herder, J.-W.A., Bautz, M. (eds.) Space Telescopes and Instrumentation 2014: Ultraviolet to Gamma Ray, vol. 9144, p. 914420. SPIE, ??? (2014). https://doi.org/10.1117/12.2056811. International Society for Optics and Photonics. https://doi.org/10.1117/12.2056811

[30] Harrison, F.A., Craig, W.W., Christensen, F.E., Hailey, C.J., Zhang, W.W., Boggs, S.E., Stern, D., Cook, W.R., Forster, K., Giommi, P., Grefenstette, B.W., Kim, Y., Kitaguchi, T., Koglin, J.E., Madsen, K.K., Mao, P.H., Miyasaka, H., Mori, K., Perri, M., Pivovaroff, M.J., Puccetti, S., Rana, V.R., Westergaard, N.J., Willis, J., Zoglauer, A., An, H., Bachetti, M., Barrière, N.M., Bellm, E.C., Bhalerao, V., Brejnholt, N.F., Fuerst, F., Liebe, C.C., Markwardt, C.B., Nynka, M., Vogel, J.K., Walton, D.J., Wik, D.R., Alexander, D.M., Cominsky, L.R., Hornschemeier, A.E., Hornstrup, A., Kaspi, V.M., Madejski, G.M., Matt, G., Molendi, S., Smith, D.M., Tomsick, J.A., Ajello, M., Ballantyne, D.R., Baloković, M., Barret, D., Bauer, F.E., Blandford, R.D., Brandt, W.N., Brenneman, L.W., Chiang, J., Chakrabarty, D., Chenevez, J., Comastri, A., Dufour, F., Elvis, M., Fabian, A.C., Farrah, D., Fryer, C.L., Gotthelf, E.V., Grindlay, J.E., Helfand, D.J., Krivonos, R., Meier, D.L., Miller, J.M., Natalucci, L., Ogle, P., Ofek, E.O., Ptak, A., Reynolds, S.P.,

Rigby, J.R., Tagliaferri, G., Thorsett, S.E., Treister, E., Urry, C.M.: The Nuclear Spectroscopic Telescope Array (NuSTAR) High-energy X-Ray Mission. ApJ **770**(2), 103 (2013) arXiv:1301.7307 [astro-ph.IM]. https://doi.org/10.1088/0004-637X/770/2/103

[31] Done, C., Gierliński, M., Kubota, A.: Modelling the behaviour of accretion flows in x-ray binaries. The Astronomy and Astrophysics Review **15**(1), 1–66 (2007). https://doi.org/10.1007/s00159-007-0006-1

[32] Connors, R.M.T., García, J.A., Tomsick, J., Hare, J., Dauser, T., Grinberg, V., Steiner, J.F., Mastroserio, G., Sridhar, N., Fabian, A.C., Jiang, J., Parker, M.L., Harrison, F., Kallman, T.R.: Reflection Modeling of the Black Hole Binary 4U 1630-47: The Disk Density and Returning Radiation. ApJ **909**(2), 146 (2021) arXiv:2101.06343 [astro-ph.HE]. https://doi.org/10.3847/1538-4357/abdd2c

[33] Chandrasekhar, S.: Radiative Transfer. Dover, New York (1960)

[34] Stark, R.F., Connors, P.A.: Observational test for the existence of a rotating black hole in Cyg X-1. Nature **266**(5601), 429–430 (1977). https://doi.org/10.1038/266429a0

[35] Dovčiak, M., Muleri, F., Goosmann, R.W., Karas, V., Matt, G.: Thermal disc emission from a rotating black hole: X-ray polarization signatures. MNRAS **391**(1), 32–38 (2008) arXiv:0809.0418 [astro-ph]. https://doi.org/10.1111/j.1365-2966.2008.13872.x

[36] Schnittman, J.D., Krolik, J.H.: X-ray Polarization from Accreting Black Holes: The Thermal State. ApJ **701**(2), 1175–1187 (2009) arXiv:0902.3982 [astro-ph.HE]. https://doi.org/10.1088/0004-637X/701/2/1175

[37] Taverna, R., Zhang, W., Dovčiak, M., Bianchi, S., Bursa, M., Karas, V., Matt, G.: Towards a complete description of spectra and polarization of black hole accretion discs: albedo profiles and returning radiation. MNRAS **493**(4), 4960–4977 (2020) https://academic.oup.com/mnras/article-pdf/493/4/4960/32955882/staa598.pdf. https://doi.org/10.1093/mnras/staa598

[38] Taverna, R., Marra, L., Bianchi, S., Dovčiak, M., Goosmann, R., Marin, F., Matt, G., Zhang, W.: Spectral and polarization properties of black hole accretion disc emission: including absorption effects. MNRAS **501**(3), 3393–3405 (2021) arXiv:2012.06504 [astro-ph.HE]. https://doi.org/10.1093/mnras/staa3859

[39] Podgorný, J., Dovčiak, M., Marin, F., Goosmann, R., Różańska, A.: Spectral and polarization properties of reflected X-ray emission from black hole accretion discs. MNRAS **510**(4), 4723–4735 (2022) arXiv:2201.07494 [astro-ph.HE]. https://doi.org/10.1093/mnras/stab3714

[40] Blandford, R.D., Payne, D.G.: Hydromagnetic flows from accretion disks and the production of radio jets. MNRAS **199**, 883–903 (1982). https://doi.org/10.1093/mnras/199.4.883

[41] Contopoulos, J.: Magnetically Driven Relativistic Jets and Winds: Exact Solutions. ApJ **432**, 508 (1994). https://doi.org/10.1086/174590

[42] Ferreira, J.: Magnetically-driven jets from Keplerian accretion discs. A&A **319**, 340–359 (1997) arXiv:astro-ph/9607057 [astro-ph]. https://doi.org/10.48550/arXiv.astro-ph/9607057

[43] Fukumura, K., Kazanas, D., Contopoulos, I., Behar, E.: Magnetohydrodynamic Accretion Disk Winds as X-ray Absorbers in Active Galactic Nuclei. ApJ **715**(1), 636–650 (2010) arXiv:0910.3001 [astro-ph.HE]. https://doi.org/10.1088/0004-637X/715/1/636

[44] Chakravorty, S., Petrucci, P.-O., Ferreira, J., Henri, G., Belmont, R., Clavel, M., Corbel, S., Rodriguez, J., Coriat, M., Drappeau, S., Malzac, J.: Absorption lines from magnetically driven winds in X-ray binaries. A&A **589**, 119 (2016) arXiv:1512.09149 [astro-ph.HE]. https://doi.org/10.1051/0004-6361/201527163

[45] Fukumura, K., Kazanas, D., Shrader, C., Tombesi, F., Kalapotharakos, C., Behar, E.: Modeling Magnetic Disk Wind State Transitions in Black Hole X-Ray Binaries. ApJ **912**(2), 86 (2021) arXiv:2103.05891 [astro-ph.HE]. https://doi.org/10.3847/1538-4357/abedaf

[46] Wielgus, M., Lančová, D., Straub, O., Kluźniak, W., Narayan, R., Abarca, D., Różańska, A., Vincent, F., Török, G., Abramowicz, M.: Observational properties of puffy discs: radiative GRMHD spectra of mildly sub-Eddington accretion. MNRAS **514**(1), 780–789 (2022) arXiv:2202.08831 [astro-ph.HE]. https://doi.org/10.1093/mnras/stac1317

[47] Bardeen, J.M., Petterson, J.A.: The Lense-Thirring Effect and Accretion Disks around Kerr Black Holes. Astrophys. Lett. **195**, 65 (1975). https://doi.org/10.1086/181711

[48] Kushwaha, A., Jayasurya, K.M., Agrawal, V.K., Nandi, A.: IXPE and NICER view of Black hole X-ray binary 4U 1630-47: First significant detection of polarized emission in thermal state. arXiv (2023). https://doi.org/10.48550/ARXIV.2303.05462. https://arxiv.org/abs/2303.05462

[49] Rawat, D., Garg, A., Méndez, M.: Detection of X-ray polarized emission and accretion-disk winds with IXPE and NICER in the black-hole X-ray binary 4U 1630-47. arXiv (2023). https://doi.org/10.48550/ARXIV.2303.02745. https://arxiv.org/abs/2303.02745

[50] Ratheesh, A., Matt, G., Tombesi, F., Soffitta, P., Pesce-Rollins, M., Di Marco, A.: Exploring the accretion-ejection geometry of GRS 1915+105 in the obscured state with future X-ray spectro-polarimetry. A&A **655**, 96 (2021) arXiv:2109.00419 [astro-ph.HE]. https://doi.org/10.1051/0004-6361/202140701

[51] Ramsey, B.D., Bongiorno, S.D., Kolodziejczak, J.J., Kilaru, K., Alexander, C., Baumgartner, W.H., Elsner, R.F., McCracken, J., Mitsuishi, I., Pavelitz, S.D., Ranganathan, J., Sanchez, J., Speegle, C.O., Weddendorf, B., O'Dell, S.L.: IXPE mirror module assemblies. In: O'Dell, S.L., Pareschi, G. (eds.) Optics for EUV, X-Ray, and Gamma-Ray Astronomy IX. Society of Photo-Optical Instrumentation Engineers (SPIE) Conference Series, vol. 11119, p. 1111903 (2019). https://doi.org/10.1117/12.2531956

[52] Soffitta, P., Baldini, L., Bellazzini, R., Costa, E., Latronico, L., Muleri, F., Del Monte, E., Fabiani, S., Minuti, M., Pinchera, M., Sgro', C., Spandre, G., Trois, A., Amici, F., Andersson, H., Attina', P., Bachetti, M., Barbanera, M., Borotto, F., Brez, A., Brienza, D., Caporale, C., Cardelli, C., Carpentiero, R., Castellano, S., Castronuovo, M., Cavalli, L., Cavazzuti, E., Ceccanti, M., Centrone, M., Ciprini, S., Citraro, S., D'Amico, F., D'Alba, E., Di Cosimo, S., Di Lalla, N., Di Marco, A., Di Persio, G., Donnarumma, I., Evangelista, Y., Ferrazzoli, R., Hayato, A., Kitaguchi, T., La Monaca, F., Lefevre, C., Loffredo, P., Lorenzi, P., Lucchesi, L., Magazzu, C., Maldera, S., Manfreda, A., Mangraviti, E., Marengo, M., Matt, G., Mereu, P., Morbidini, A., Mosti, F., Nakano, T., Nasimi, H., Negri, B., Nenonen, S., Nuti, A., Orsini, L., Perri, M., Pesce-Rollins, M., Piazzolla, R., Pilia, M., Profeti, A., Puccetti, S., Rankin, J., Ratheesh, A., Rubini, A., Santoli, F., Sarra, P., Scalise, E., Sciortino, A., Tamagawa, T., Tardiola, M., Tobia, A., Vimercati, M., Xie, F.: The Instrument of the Imaging X-Ray Polarimetry Explorer. AJ **162**(5), 208 (2021) arXiv:2108.00284 [astro-ph.IM]. https://doi.org/10.3847/1538-3881/ac19b0

[53] Baldini, L., Barbanera, M., Bellazzini, R., Bonino, R., Borotto, F., Brez, A., Caporale, C., Cardelli, C., Castellano, S., Ceccanti, M., Citraro, S., Di Lalla, N., Latronico, L., Lucchesi, L., Magazzù, C., Magazzù, G., Maldera, S., Manfreda, A., Marengo, M., Marrocchesi, A., Mereu, P., Minuti, M., Mosti, F., Nasimi, H., Nuti, A., Oppedisano, C., Orsini, L., Pesce-Rollins, M., Pinchera, M., Profeti, A., Sgrò, C., Spandre, G., Tardiola, M., Zanetti, D., Amici, F., Andersson, H., Attinà, P., Bachetti, M., Baumgartner, W., Brienza, D., Carpentiero, R., Castronuovo, M., Cavalli, L., Cavazzuti, E.,

Centrone, M., Costa, E., D'Alba, E., D'Amico, F., Del Monte, E., Di Cosimo, S., Di Marco, A., Di Persio, G., Donnarumma, I., Evangelista, Y., Fabiani, S., Ferrazzoli, R., Kitaguchi, T., La Monaca, F., Lefevre, C., Loffredo, P., Lorenzi, P., Mangraviti, E., Matt, G., Meilahti, T., Morbidini, A., Muleri, F., Nakano, T., Negri, B., Nenonen, S., O'Dell, S.L., Perri, M., Piazzolla, R., Pieraccini, S., Pilia, M., Puccetti, S., Ramsey, B.D., Rankin, J., Ratheesh, A., Rubini, A., Santoli, F., Sarra, P., Scalise, E., Sciortino, A., Soffitta, P., Tamagawa, T., Tennant, A.F., Tobia, A., Trois, A., Uchiyama, K., Vimercati, M., Weisskopf, M.C., Xie, F., Zanetti, F., Zhou, Y.: Design, construction, and test of the Gas Pixel Detectors for the IXPE mission. Astroparticle Physics **133**, 102628 (2021) arXiv:2107.05496 [astro-ph.IM]. https://doi.org/10.1016/j.astropartphys.2021.102628

[54] Joye, W.A., Mandel, E.: New Features of SAOImage DS9. In: Payne, H.E., Jedrzejewski, R.I., Hook, R.N. (eds.) Astronomical Data Analysis Software and Systems XII. Astronomical Society of the Pacific Conference Series, vol. 295, p. 489 (2003)

[55] Nasa High Energy Astrophysics Science Archive Research Center (Heasarc): HEAsoft: Unified Release of FTOOLS and XANADU. Astrophysics Source Code Library, record ascl:1408.004 (2014)

[56] Arnaud, K.A.: XSPEC: The First Ten Years. In: Jacoby, G.H., Barnes, J. (eds.) Astronomical Data Analysis Software and Systems V. Astronomical Society of the Pacific Conference Series, vol. 101, p. 17 (1996)

[57] Gendreau, K.C., Arzoumanian, Z., Adkins, P.W., Albert, C.L., Anders, J.F., Aylward, A.T., Baker, C.L., Balsamo, E.R., Bamford, W.A., Benegalrao, S.S., Berry, D.L., Bhalwani, S., Black, J.K., Blaurock, C., Bronke, G.M., Brown, G.L., Budinoff, J.G., Cantwell, J.D., Cazeau, T., Chen, P.T., Clement, T.G., Colangelo, A.T., Coleman, J.S., Coopersmith, J.D., Dehaven, W.E., Doty, J.P., Egan, M.D., Enoto, T., Fan, T.W., Ferro, D.M., Foster, R., Galassi, N.M., Gallo, L.D., Green, C.M., Grosh, D., Ha, K.Q., Hasouneh, M.A., Heefner, K.B., Hestnes, P., Hoge, L.J., Jacobs, T.M., Jørgensen, J.L., Kaiser, M.A., Kellogg, J.W., Kenyon, S.J., Koenecke, R.G., Kozon, R.P., LaMarr, B., Lambertson, M.D., Larson, A.M., Lentine, S., Lewis, J.H., Lilly, M.G., Liu, K.A., Malonis, A., Manthripragada, S.S., Markwardt, C.B., Matonak, B.D., Mcginnis, I.E., Miller, R.L., Mitchell, A.L., Mitchell, J.W., Mohammed, J.S., Monroe, C.A., Montt de Garcia, K.M., Mulé, P.D., Nagao, L.T., Ngo, S.N., Norris, E.D., Norwood, D.A., Novotka, J., Okajima, T., Olsen, L.G., Onyeachu, C.O., Orosco, H.Y., Peterson, J.R., Pevear, K.N., Pham, K.K., Pollard, S.E., Pope, J.S., Powers, D.F., Powers, C.E., Price, S.R., Prigozhin, G.Y., Ramirez, J.B., Reid, W.J., Remillard, R.A., Rogstad, E.M., Rosecrans, G.P., Rowe, J.N., Sager, J.A., Sanders, C.A., Savadkin, B., Saylor, M.R., Schaeffer, A.F., Schweiss, N.S., Semper, S.R., Serlemitsos, P.J., Shackelford, L.V., Soong,

Y., Struebel, J., Vezie, M.L., Villasenor, J.S., Winternitz, L.B., Wofford, G.I., Wright, M.R., Yang, M.Y., Yu, W.H.: The Neutron star Interior Composition Explorer (NICER): design and development. In: den Herder, J.-W.A., Takahashi, T., Bautz, M. (eds.) Space Telescopes and Instrumentation 2016: Ultraviolet to Gamma Ray. Society of Photo-Optical Instrumentation Engineers (SPIE) Conference Series, vol. 9905, p. 99051 (2016). https://doi.org/10.1117/12.2231304

[58] Remillard, R.A., Loewenstein, M., Steiner, J.F., Prigozhin, G.Y., LaMarr, B., Enoto, T., Gendreau, K.C., Arzoumanian, Z., Markwardt, C., Basak, A., Stevens, A.L., Ray, P.S., Altamirano, D., Buisson, D.J.K.: An Empirical Background Model for the NICER X-Ray Timing Instrument. AJ **163**(3), 130 (2022) arXiv:2105.09901 [astro-ph.IM]. https://doi.org/10.3847/1538-3881/ac4ae6

[59] Kaastra, J.S., Bleeker, J.A.M.: Optimal binning of X-ray spectra and response matrix design. A&A **587**, 151 (2016) arXiv:1601.05309 [astro-ph.IM]. https://doi.org/10.1051/0004-6361/201527395

[60] Li, L.-X., Zimmerman, E.R., Narayan, R., McClintock, J.E.: Multitemperature Blackbody Spectrum of a Thin Accretion Disk around a Kerr Black Hole: Model Computations and Comparison with Observations. ApJS **157**(2), 335–370 (2005) arXiv:astro-ph/0411583 [astro-ph]. https://doi.org/10.1086/428089

[61] Zdziarski, A.A., Johnson, W.N., Magdziarz, P.: Broad-band γ-ray and X-ray spectra of NGC 4151 and their implications for physical processes and geometry. MNRAS **283**(1), 193–206 (1996) arXiv:astro-ph/9607015 [astro-ph]. https://doi.org/10.1093/mnras/283.1.193

[62] Życki, P.T., Done, C., Smith, D.A.: The 1989 May outburst of the soft X-ray transient GS 2023+338 (V404 Cyg). MNRAS **309**(3), 561–575 (1999) arXiv:astro-ph/9904304 [astro-ph]. https://doi.org/10.1046/j.1365-8711.1999.02885.x

[63] Ferland, G.J., Chatzikos, M., Guzmán, F., Lykins, M.L., van Hoof, P.A.M., Williams, R.J.R., Abel, N.P., Badnell, N.R., Keenan, F.P., Porter, R.L., Stancil, P.C.: The 2017 Release Cloudy. Rev. Mex. Astron. Astrofis. **53**, 385–438 (2017) arXiv:1705.10877 [astro-ph.GA]

[64] Wilms, J., Allen, A., McCray, R.: On the Absorption of X-Rays in the Interstellar Medium. ApJ **542**(2), 914–924 (2000) arXiv:astro-ph/0008425 [astro-ph]. https://doi.org/10.1086/317016

[65] Wang, J., Mastroserio, G., Kara, E., García, J.A., Ingram, A., Connors, R., van der Klis, M., Dauser, T., Steiner, J.F., Buisson, D.J.K., Homan, J., Lucchini, M., Fabian, A.C., Bright, J., Fender, R., Cackett,

E.M., Remillard, R.A.: Disk, Corona, Jet Connection in the Intermediate State of MAXI J1820+070 Revealed by NICER Spectral-timing Analysis. Astrophys. Lett. **910**(1), 3 (2021) arXiv:2103.05616 [astro-ph.HE]. https://doi.org/10.3847/2041-8213/abec79

[66] Podgorny, J., Marra, L., Muleri, F., Rodriguez Cavero, N., Ratheesh, A., Dovciak, M., Mikusincova, R., Brigitte, M., Steiner, J.F., Veledina, A., Bianchi, S., Krawczynski, H., Svoboda, J., Kaaret, P., Matt, G., Garcia, J.A., Petrucci, P.-O., Lutovinov, A.A., Semena, A.N., Di Marco, A., Negro, M., Weisskopf, M.C., Ingram, A., Poutanen, J., Beheshtipour, B., Chun, S., Hu, K., Mizuno, T., Sixuan, Z., Tombesi, F., Zane, S., Agudo, I., Antonelli, L.A., Bachetti, M., Baldini, L., Baumgartner, W.H., Bellazzini, R., Bongiorno, S.D., Bonino, R., Brez, A., Bucciantini, N., Capitanio, F., Castellano, S., Cavazzuti, E., Chen, C.-T., Ciprini, S., Costa, E., De Rosa, A., Del Monte, E., Di Gesu, L., Di Lalla, N., Donnarumma, I., Doroshenko, V., Ehlert, S.R., Enoto, T., Evangelista, Y., Fabiani, S., Ferrazzoli, R., Gunji, S., Hayashida, K., Heyl, J., Iwakiri, W., Jorstad, S.G., Karas, V., Kislat, F., Kitaguchi, T., Kolodziejczak, J.J., La Monaca, F., Latronico, L., Liodakis, I., Maldera, S., Manfreda, A., Marin, F., Marinucci, A., Marscher, A.P., Marshall, H.L., Massaro, F., Mitsuishi, I., Ng, C.-Y., O'Dell, S.L., Omodei, N., Oppedisano, C., Papitto, A., Pavlov, G.G., Peirson, A.L., Perri, M., Pesce-Rollins, M., Pilia, M., Possenti, A., Puccetti, S., Ramsey, B.D., Rankin, J., Roberts, O.J., Romani, R.W., Sgro, C., Slane, P., Soffitta, P., Spandre, G., Swartz, D.A., Tamagawa, T., Tavecchio, F., Taverna, R., Tawara, Y., Tennant, A.F., Thomas, N.E., Trois, A., Tsygankov, S.S., Turolla, R., Vink, J., Wu, K., Xie, F.: The first X-ray polarimetric observation of the black hole binary LMC X-1. arXiv e-prints, 2303–12034 (2023) arXiv:2303.12034 [astro-ph.HE]. https://doi.org/10.48550/arXiv.2303.12034

[67] Seifina, E., Titarchuk, L., Shaposhnikov, N.: Black Hole Mass Determination in the X-Ray Binary 4U 1630-47: Scaling of Spectral and Variability Characteristics. ApJ **789**(1), 57 (2014) arXiv:1405.4711 [astro-ph.SR]. https://doi.org/10.1088/0004-637X/789/1/57

[68] Sądowski, A.: Slim accretion disks around black holes. arXiv e-prints, 1108–0396 (2011) arXiv:1108.0396 [astro-ph.HE]. https://doi.org/10.48550/arXiv.1108.0396

[69] Hubeny, I., Hubeny, V.: Non-LTE Models and Theoretical Spectra of Accretion Disks in Active Galactic Nuclei. II. Vertical Structure of the Disk. ApJ **505**(2), 558–576 (1998) arXiv:astro-ph/9804288 [astro-ph]. https://doi.org/10.1086/306207

[70] Straub, O., Bursa, M., Sądowski, A., Steiner, J.F., Abramowicz, M.A.,

Kluźniak, W., McClintock, J.E., Narayan, R., Remillard, R.A.: Testing slim-disk models on the thermal spectra of LMC X-3. A&A **533**, 67 (2011) arXiv:1106.0009 [astro-ph.SR]. https://doi.org/10.1051/0004-6361/201117385

[71] Zimmerman, E.R., Narayan, R., McClintock, J.E., Miller, J.M.: Multitemperature Blackbody Spectra of Thin Accretion Disks with and without a Zero-Torque Inner Boundary Condition. ApJ **618**(2), 832–844 (2005) arXiv:astro-ph/0408209 [astro-ph]. https://doi.org/10.1086/426071

[72] Sobolev, V.V.: On the polarization of scattered light. Uch. Zap. Leningrad Univ. **16** (1949)

[73] Chandrasekhar, S.: Radiative Transfer. Dover Publications, New York (1960)

[74] de Jong, J.A., van Paradijs, J., Augusteijn, T.: Reprocessing of X rays in low-mass X-ray binaries. A&A **314**, 484–490 (1996)

[75] Lightman, A.P., Shapiro, S.L.: Spectrum and polarization of X-rays from accretion disks around black holes. Astrophys. Lett. **198**, 73–75 (1975). https://doi.org/10.1086/181815

[76] Loskutov, V.M., Sobolev, V.V.: Polarization of scattered light in atmospheres with embedded sources. Astrofizika **15**, 241–252 (1979)

[77] Milne, E.A.: Radiative equilibrium in the outer layers of a star. MNRAS **81**, 361–375 (1921). https://doi.org/10.1093/mnras/81.5.361

[78] Loskutov, V.M., Sobolev, V.V.: Polarization of radiation scattered by an inhomogeneous atmosphere. Astrofizika **17**, 97–108 (1981)

[79] Dumont, A.-M., Collin, S., Paletou, F., Coupé, S., Godet, O., Pelat, D.: Escape probability methods versus "exact" transfer for modelling the X-ray spectrum of Active Galactic Nuclei and X-ray binaries. A&A **407**, 13–30 (2003). https://doi.org/10.1051/0004-6361:20030890

[80] Goosmann, R.W., Gaskell, C.M.: Modeling optical and UV polarization of AGNs. I. Imprints of individual scattering regions. A&A **465**(1), 129–145 (2007) arXiv:astro-ph/0507072 [astro-ph]. https://doi.org/10.1051/0004-6361:20053555

[81] Marin, F., Goosmann, R.W., Gaskell, C.M., Porquet, D., Dovčiak, M.: Modeling optical and UV polarization of AGNs. II. Polarization imaging and complex reprocessing. A&A **548**, 121 (2012) arXiv:1209.2915 [astro-ph.HE]. https://doi.org/10.1051/0004-6361/201219751

[82] Marin, F., Goosmann, R.W., Gaskell, C.M.: Modeling optical and UV polarization of AGNs. III. From uniform-density to clumpy regions. A&A **577**, 66 (2015) arXiv:1503.05311 [astro-ph.HE]. https://doi.org/10.1051/0004-6361/201525628

[83] Marin, F.: Modeling optical and UV polarization of AGNs. V. Dilution by interstellar polarization and the host galaxy. A&A **615**, 171 (2018) arXiv:1805.09098 [astro-ph.HE]. https://doi.org/10.1051/0004-6361/201833225

[84] Davis, S.W., Blaes, O.M., Hubeny, I., Turner, N.J.: Relativistic Accretion Disk Models of High-State Black Hole X-Ray Binary Spectra. ApJ **621**(1), 372–387 (2005) arXiv:astro-ph/0408590 [astro-ph]. https://doi.org/10.1086/427278

[85] Różańska, A., Madej, J., Konorski, P., Sądowski, A.: Iron lines in model disk spectra of Galactic black hole binaries. A&A **527**, 47 (2011) arXiv:1011.2061 [astro-ph.HE]. https://doi.org/10.1051/0004-6361/201015626

[86] Asplund, M., Grevesse, N., Sauval, A.J.: The Solar Chemical Composition. In: Barnes, I. Thomas G., Bash, F.N. (eds.) Cosmic Abundances as Records of Stellar Evolution and Nucleosynthesis. Astronomical Society of the Pacific Conference Series, vol. 336, p. 25 (2005)

[87] Rybicki, G.B., Lightman, A.P.: Radiative Processes in Astrophysics, (1979)

[88] Suleimanov, V.F., Ghosh, K.K., Austin, R.A., Ramsey, B.D.: X-ray Emission from Accretion Disks in Active Galactic Nuclei. Astronomy Letters **28**(11), 745–754 (2002). https://doi.org/10.1134/1.1518712

[89] Suleimanov, V.F., Lipunova, G.V., Shakura, N.I.: The thickness of accretion α-disks: Theory and observations. Astronomy Reports **51**(7), 549–562 (2007). https://doi.org/10.1134/S1063772907070049

[90] Riffert, H., Herold, H.: Relativistic Accretion Disk Structure Revisited. ApJ **450**, 508 (1995). https://doi.org/10.1086/176161

[91] Suleymanov, V.F.: Modeling of accretion disks and spectra of radiation in cataclysmic variable stars. I. V603 Aql. Soviet Astronomy Letters **18**, 104 (1992)

[92] Suleimanov, V.F., Poutanen, J., Doroshenko, V., Werner, K.: Expected polarization properties of nonmagnetized CCOs. arXiv e-prints, 2303–01382 (2023) arXiv:2303.01382 [astro-ph.HE]. https://doi.org/10.48550/arXiv.2303.01382

[93] Asplund, M., Grevesse, N., Sauval, A.J., Scott, P.: The Chemical Composition of the Sun. ARA&A **47**(1), 481–522 (2009) arXiv:0909.0948 [astro-ph.SR]. https://doi.org/10.1146/annurev.astro.46.060407.145222

[94] Hubeny, I., Hummer, D.G., Lanz, T.: NLTE model stellar atmospheres with line blanketing near the series limits. A&A **282**, 151–167 (1994)

[95] Mikusincova, R., Dovciak, M., Bursa, M., Lalla, N.D., Matt, G., Svoboda, J., Taverna, R., Zhang, W.: X-ray polarimetry as a tool to measure the black hole spin in microquasars: simulations of IXPE capabilities. MNRAS **519**(4), 6138–6148 (2023) arXiv:2301.04002 [astro-ph.HE]. https://doi.org/10.1093/mnras/stad077

[96] West, A., Krawczynski, H.: Impact of the Accretion Disk Thickness on the Polarization of the Thermal Emission from Stellar Mass Black Holes. ApJ(2023)

[97] Page, D.N., Thorne, K.S.: Disk-Accretion onto a Black Hole. Time-Averaged Structure of Accretion Disk. ApJ **191**, 499–506 (1974). https://doi.org/10.1086/152990

References [1] – [50] are for the main section, while the rest are for the Methods section.